The long activations of α2 glycine channels can be described by a mechanism with reaction intermediates ("flip")

Paraskevi Krashia, Remigijus Lape, Francesco Lodesani, David Colquhoun, and Lucia G. Sivilotti

Department of Neuroscience, Physiology and Pharmacology, University College London, London WC1E 6BT, England, UK

The α2 glycine receptor (GlyR) subunit, abundant in embryonic neurons, is replaced by α1 in the adult nervous system. The single-channel activity of homomeric α2 channels differs from that of α1-containing GlyRs, as even at the lowest glycine concentration (20 µM), openings occurred in long (>300-ms) groups with high open probability (P_{open}; 0.96; cell-attached recordings, HEK-expressed channels). Shut-time intervals within groups of openings were dominated by short shuttings of 5–10 µs. The lack of concentration dependence in the groups of openings suggests that they represent single activations, separated by very long shut times at low concentrations. Several putative mechanisms were fitted by maximizing the likelihood of the entire sequence of open and shut times, with exact missed-events allowance (program HJCFIT). Records obtained at several glycine concentrations were fitted simultaneously. The adequacy of the different schemes was judged by the accuracy with which they predicted not only single-channel data but also the time course and concentration dependence of macroscopic responses elicited by rapid glycine applications to outside-out patches. The data were adequately described only with schemes incorporating a reaction intermediate in the activation, and the best was a flip mechanism with two binding sites and one open state. Fits with this mechanism showed that for α2 channels, the opening rate constant is very fast, ~130,000 s^{-1}, much as for α1β GlyRs (the receptor in mature synapses), but the estimated true mean open time is 20 times longer (around 3 ms). The efficacy for the flipping step and the binding affinity were lower for α2 than for α1β channels, but the overall efficacies were similar. As we previously showed for α1 homomeric receptors, in α2 glycine channels, maximum P_{open} is achieved when fewer than all five of the putative binding sites in the pentamer are occupied by glycine.

INTRODUCTION

Out of the four known isoforms of the glycine receptor (GlyR) α subunit, α2 (Grenningloh et al., 1990; Akagi et al., 1991) may play a major role in the embryonic form of GlyRs (Legendre, 2001), as its transcripts, abundant in the embryonic and neonatal rat, are gradually replaced by α1 in the adult (Akagi et al., 1991; Malosio et al., 1991; Watanabe and Akagi, 1995). This is supported by a variety of functional observations. Takahashi et al. (1992) observed longer apparent open times in recombinant α2 versus α1 GlyRs, and in embryonic versus adult rat spinal GlyRs. The decay of glycinergic IPSCs also speeds up with development. The simplest explanation is that embryonic and neonatal GlyRs contain mostly α2 subunits, whereas adult receptors are α1β heteromers (Becker et al., 1988; Langosch et al., 1988; Hoch et al., 1989). Nevertheless, it is far from certain that the slow glycinergic synaptic currents observed early in development are mediated by α2 homomeric receptors. Homomeric GlyRs probably cannot cluster at the synapse, because only β subunits can interact with gephyrin (Meyer et al., 1995). Second, α2 is expressed in areas where no glycine-mediated synaptic transmission has been detected (Flint et al., 1998; Mangin et al., 2002) and by nonneuronal cells, such as glial or progenitor cells (Belachew et al., 1998; Nguyen et al., 2002). Mangin et al. (2003) showed that α2 homomeric receptors are unsuitable for fast synaptic transmission because they activate and deactivate slowly and have a low probability of opening in response to the rapid application of brief glycine pulses (Mangin et al., 2003). It has therefore been suggested that α2 homomeric receptors may be mainly extrasynaptic and that they can be activated by a paracrine-like release of glycine or taurine during neuronal development (Legendre, 2001; Clements, 2002; Mangin et al., 2003). In addition to that, synaptic currents recorded in neonatal hypoglossal motoneurons decay almost 10 times faster than currents elicited on recombinant α2 channels (Mangin et al., 2003), leading Singer et al. (1998) to suggest that they are mediated by α2β heteromeric GlyR.

P. Krashia and R. Lape contributed equally to this paper.

Correspondence to Lucia G. Sivilotti: l.sivilotti@ucl.ac.uk

F. Lodesani's present address is Advanced Center for Electronic Systems ARCES II School of Engineering, University of Bologna, 40125 Bologna, Italy.

Abbreviation used in this paper: GlyR, glycine receptor; n_H, Hill coefficient; P_{open}, open probability.

Global fitting of kinetic models to single-channel data from recombinant α1-containing GlyRs led us to describe an activation mechanism ("flip") that explicitly incorporates intermediate shut states between agonist binding and channel opening (Burzomato et al., 2004). Mechanisms that include pre-open shut states such as flip states, or for muscle nicotinic receptors, "primed" states (Mukhtasimova et al., 2009), are attractive because they offer a suggestive kinetic parallel to the events that are likely to happen in the extracellular domain before channel opening, such as domain closing and/or C-loop capping. In addition to that, they have been found to describe well channel activation for a variety of wild-type and mutant subunit combinations for glycine, muscle nicotinic, and GABA_A receptors, notably with respect to the differences between full and partial agonists in the nicotinic superfamily and to the complex structure of unliganded openings in gain-of-function mutants (Burzomato et al., 2004; Plested et al., 2007; Lape et al., 2008; Mukhtasimova et al., 2009; Keramidas and Harrison, 2010). Our aim in the present work was to extend this approach to recombinant α2 GlyRs, to establish a quantitative activation mechanism for this channel, and to test whether a flip-type mechanism could provide an adequate description for both single-channel and macroscopic data from recombinant α2 homomers. For the first time in fitting GlyR channel activity, we found that a flip-type mechanism describes the data somewhat better than a less constrained mechanism incorporating distal shut states (such as the mechanism proposed by Jones and Westbrook, 1995).

MATERIALS AND METHODS

GlyR α2 subunit cDNA construct, HEK293 cell culture, and transfection

HEK293 cells (American Type Culture Collection and LGC Standards) were maintained in a humidified incubator at 37°C (95% air/5% CO_2) in Dulbecco's modified Eagle's medium supplemented with: sodium pyruvate (0.11 g/liter), heat-inactivated fetal bovine serum (10% vol/vol), and penicillin G (100 U/ml)/streptomycin sulfate (100 µg/ml; all from Invitrogen). Cells were passaged every 2–3 d, up to 30 times. Cells were plated on glass coverslips (13-mm diameter, sterilized over flame), placed in 35-mm sterile Petri dishes containing 1.5–2 ml Dulbecco's modified Eagle's medium, 4–6 h before transfection, to allow cells to attach. Cells used for fast concentration jumps were plated onto coverslips coated with poly-L-lysine (Sigma-Aldrich) by incubation of the coverslips for ~40 min, followed by washing with autoclaved water and oven drying at 60°C.

HEK293 cells were transiently transfected with the rat GlyR α2 cDNA (Isoform A; available from GenBank/EMBL/DDBJ under accession no. AJ310837; full-length sequence verified) in the pcDNA3.1 vector. Transfection was by calcium phosphate–DNA coprecipitation (Groot-Kormelink et al., 2002). In brief, cDNA was added to $CaCl_2$ solution (340 mM in sterile water) at a volume ratio of 1:5, and this mixture was added drop-by-drop to an equal volume of 2× Hank's buffered saline (280 mM NaCl, 2.8 mM Na_2HPO_4, and 50 mM HEPES, pH 7.2 with NaOH) to form the precipitate. The final mixture was then added dropwise over the plated cells. The cDNA used for transfection contained 3–20% α2/pcDNA3.1, 18% pEGFP-c1, and 62–79% pcDNA3.1 vector lacking the α2 coding sequence. Adding empty vector was found to be important for the health of the transfected cells and to ensure that the level of α2 GlyR expression was optimal for recording. The total amount of the final cDNA mixture per plate was kept constant at 3 µg. Recordings were performed 2–3 h after washing and no more than 3 d after transfection. We attempted to obtain single-channel recordings also from α2β heteromeric GlyR, but the expression level was consistently too low, despite considerable effort to improve it.

Single-channel recording

Cell-attached single-channel currents were recorded at 19–21°C with thick-walled borosilicate pipettes (with filament; Harvard Apparatus) coated near the tip with Sylgard (Dow Corning) and fire-polished before use to a final resistance of 5–12 MΩ. Electrodes were filled with extracellular medium (in mM: 20 Na-gluconate, 102.7 NaCl, 2 KCl, 2 $CaCl_2$, 1.2 $MgCl_2$, 10 HEPES, 20 TEA-Cl, 15 sucrose, and 14 glucose, pH 7.4 with NaOH; osmolarity 320 mOsm) plus the appropriate concentration of glycine. All solutions were prepared in HPLC-grade water (VWR International) to minimize contamination by glycine and filtered through a 0.2-µm Cyclopore track-etched membrane (GE Healthcare) to remove impurities that can block electrodes or affect the quality of the seal. The bath level was kept low to reduce noise.

Currents were recorded with an amplifier (Axopatch 200B; MDS Analytical Technologies) at a pipette potential of +100 mV, with no correction for junction potential, as this is calculated to be at most +1 mV (Clampex 9; MDS Analytical Technologies). Single-channel currents were prefiltered at 10 kHz by the amplifier's four-pole Bessel filter and saved on a digital audio tape with a recorder (DRA-200; Bio-Logic). Recordings were replayed, filtered at 5 or 7 kHz, and sampled at 50 or 71.43 kHz, respectively, depending on the signal-to-noise ratio, with a Digidata 1322A and Clampex software (MDS Analytical Technologies).

Single-channel current analysis

Single-channel currents were idealized by time-course fitting (SCAN program). Segments showing drifts in the baseline, seal breakdowns, or dubious channel openings were excluded, and adjacent intervals were marked unusable as appropriate. After imposing a resolution of 20–25 µs (for both shut and open times), the number of resolved time intervals (sum of shut-time and open-period intervals) ranged from 498 to 2,368 in the 12 patches used in the maximum likelihood fits.

Idealized current amplitudes longer than twice the filter rise time (66 µs at 5 kHz) were plotted as an amplitude histogram (EKDIST program). The main conductance level accounted for >99% of all fitted open intervals, so we pooled together all openings for kinetic analysis. The average amplitude of openings to the main conductance level was 5.9 ± 0.2 pA ($n = 25$ patches) but varied considerably, ranging from 4.5 to 9.1 pA. In the 12 patches used in our analysis, the range of mean amplitudes was 4.9–8.0 pA (6.1 ± 0.3 pA). This variability in amplitude was expected for cell-attached records because it will be affected by the intracellular chloride concentration and the resting membrane potential, both of which vary from cell to cell. Variability in the intracellular chloride concentration and in the true transmembrane potential is a source of error in so far as it affects the rate constant values in receptor activation.

The distributions of apparent shut times and open periods were fitted with a mixture of exponential probability density functions. Each open period was defined as the duration of time for which the channel remained continuously open, regardless of amplitude; that is, the time between two adjacent shut times that were both longer than the imposed resolution.

The true number of the channels in each patch is unknown, but for kinetic analysis, it is essential to isolate stretches of openings that are likely to arise from one individual channel. This was done in the initial stage of the analysis by fitting shut-time distributions with EKDIST to determine a critical shut time (t_{crit}) that would allow us to divide the record into true one-channel stretches of openings. Fits to the distributions obtained at EKDIST are only descriptive and not mechanism dependent; hence, parameters estimated by EKDIST were not used further in the analysis. The criterion for a group of openings to be judged to have come from one individual channel is essentially that the probability of being open within the groups is high enough that we can be almost certain that a double opening would be seen if more than one channel were present (Colquhoun and Hawkes, 1990). Groups with fewer than 10 open periods were excluded. For fitting, we tested different values of t_{crit} (with or without the use of Colquhoun-Hawkes-Srodzinski vectors; see below). We found that the most consistent fits were obtained when we used the t_{crit} values reported in the Results.

For kinetic analysis, the postulated mechanisms were evaluated using maximum likelihood fitting and the program HJCFIT. For this purpose, the idealized data from all concentrations were grouped into three independent sets, with each set containing four patches at different agonist concentrations (20 or 30 µM, 100 µM, and 1 and 10 mM glycine). All data from one set were input into the program to be fitted simultaneously to a specified mechanism, together with the resolution of 20–25 µs (the duration of the fastest event that can be detected), a t_{crit} value and the glycine concentration for each patch. The program calculates a likelihood value for the dataset from the initial guesses for the rate constant values, taking into account the imposed resolution, which is used to correct for missed events (Hawkes et al., 1990, 1992). The rate constant values are then adjusted to maximize the likelihood until a maximum is reached.

Shut times longer than t_{crit} cannot be used directly in the fitting process because they are affected by the (unknowable) number of channels in the patch. Nevertheless, some information is recoverable from the long shut times. The true (one-channel) shut time between one activation and the next is not known, but it is known that it must be at least as long as t_{crit}. This information can be used to improve the fit by replacing the normal steady-state vectors as the start and end of each group of openings, with the Colquhoun-Hawkes-Srodzinski vectors described by Colquhoun et al. (1996; Eq. 5.11). This was done for low concentration records (in this case, all concentrations except 10 mM), and simulations show that it is useful (Colquhoun et al., 2003). It cannot be used at concentrations that are high enough that desensitization occurs, because it is model dependent and our models do not include desensitized states.

We tested whether our fits were robust to the choice of initial guesses for the rate constant values to exclude the possibility of convergence to local maxima in the likelihood surface. If the fit is good and the likelihood surface has only one well-defined maximum, changing the initial guesses should not affect the estimates for the rate constants. This was not always the case, and sometimes several equivalent solutions (with similar likelihood values) were possible, suggesting that the likelihood surface was rough with several maxima. In this case, the best solution was chosen on the basis of fit quality, physical plausibility of the rate constant estimates, and predictive power of the fitted rate constants. For example, we discarded fits that gave physically impossible association rate constant values (i.e., >10^9 $M^{-1}s^{-1}$). As a test of fit quality, we used several data displays: shut-time distributions, open-period distributions, and the predicted open probability (P_{open})–concentration curve. We also used the results of the fits to simulate realizations of single-channel activity (SCSIM program) and to calculate macroscopic current relaxations to a glycine concentration jump (SCALCS program), and we compared them to our experimental observations.

All analysis programs are available from http://www.ucl.ac.uk/Pharmacology/dcpr95.html.

Macroscopic currents: recording and analysis

Macroscopic currents evoked in outside-out patches by agonist concentration pulses were recorded with thick-walled borosilicate pipettes (with filament; Harvard Apparatus), fire-polished to a final resistance of 8–15 MΩ when filled with "low [Cl^-] solution" (in mM): 121.1 K-gluconate, 1 $CaCl_2$, 1 $MgCl_2$, 10 HEPES, 11 EGTA, 6 TEA-Cl, and 2 MgATP, pH 7.2, adjusted with KOH; osmolarity 325 mOsm, adjusted with sucrose. Because of the very low Cl^- concentration in this solution, the silver/silver chloride wire of the pipette holder was re-chlorided before each experiment to compensate for the increased flow of Cl^- ions from the wire to the solution. The bath solution was the same as for single-channel recordings. All outside-out recordings were performed at a pipette holding potential of −100 mV. We did not correct for junction potential, and this gave a maximum error of +14.6 mV in low [Cl^-] solution. During the 3–5-min intervals between glycine applications, patches were held at −60 mV to prolong the stability of the seal.

Glycine, dissolved in bath solution, was applied to outside-out patches with a theta tube (Hilgenberg GmbH) cut to a final diameter of ∼150 µm at the tip. The tube was driven by a piezo stepper (Burleigh Instruments, Inc.). The exchange time was measured by the application of 30% diluted bath solution before the experiment (to optimize the electrode position) and after the rupture of the patch. Macroscopic currents were recorded with an Axopatch 200B, digitized with Digidata 1322A, and saved directly on a computer via Clampex software (5 kHz filtering, 20–50 kHz sampling rate; all from MDS Analytical Technologies).

Different glycine concentrations were applied in random order for a duration chosen to allow the current response to reach a plateau or a peak. All currents were corrected for rundown using a standard glycine concentration (about EC_{30}), which was applied every third response. Concentration–response curves were plotted using these corrected responses (averaging up to five responses), and each experiment was fitted to the Hill equation by least squares with equal weights, using the CVFIT program to get estimates of maximum current, Hill coefficient (n_H), and EC_{50}. Numbers in the text are means ± SD of the mean (SDM) from the individual fits of each experiment. For the purpose of display, responses were normalized to the fitted maximum response of the same experiment and pooled to give an average concentration–response curve.

To study the kinetics of macroscopic currents, 10–50 responses were recorded for each glycine concentration at intervals of at least 20 s to allow full recovery from desensitization (Gentet and Clements, 2002). Responses at each concentration for each patch were averaged, excluding failures or responses that contained patch breakdowns. Only experiments in which the rundown between the first and last three responses was <5% were included in the analysis. The rise time for average currents and tip potentials was measured as the time from 20 to 80% of the peak response using Clampfit 9.2 software; experiments in which the open tip response had a 20–80% exchange time slower than 300 µs were rejected. Both the time course of desensitization at prolonged glycine applications (200 ms) and the time course of deactivation at short applications (2 ms) were fitted with a sum of one or more exponentials.

RESULTS

Some definitions

For the purpose of clarity, we shall first define four terms that are used throughout to describe patterns of channel openings: group, activation, burst, and cluster.

The term "group" of openings is used as a generic description of any group of openings that is separated by short shut times, regardless of why they occur.

An "activation" is what happens between the start of the first opening of a channel until the end of the last opening before the receptor returns to the unoccupied resting state. The activation is the elementary event produced by agonist binding, consists of a burst of one or more openings that occur in quick succession, and is what underlies the deactivation rate after a macroscopic jump to zero concentration (see the appendix of Wyllie et al., 1998).

The term "burst" refers to the groups of openings that occur at very low agonist concentrations. At sufficiently low agonist concentrations, the observed bursts of openings are a close approximation to channel activations (Edmonds et al., 1995; see Discussion). The shut times between activations contain one or more sojourns in the unoccupied resting state, as well as bindings that happen not to produce an opening. They may also contain sojourns in desensitized states.

A "cluster" of openings, defined as in Sakmann et al. (1980), refers to the long groups of openings that are observed at high agonist concentrations. A cluster consists of many activations that occur in quick succession (because of the high agonist concentration), so one activation cannot be distinguished from the next one. Clusters are separated by shut times that have one or more sojourns in long-lived desensitized states. They are seen with most ligand-gated ion channels but are not easy to identify in α2 receptor records.

Properties of macroscopic currents from α2 GlyRs

To understand the α2 GlyR channel behavior in non-equilibrium conditions, we recorded macroscopic currents activated by fast application of glycine. We have recently shown (Pitt et al., 2008) that the gating of α1β GlyRs is modulated by internal Cl⁻. Channel deactivation after short glycine applications becomes faster in outside-out patches when intracellular chloride is lowered to concentrations similar to those likely to be present in the intact HEK cell (i.e., in cell-attached recordings). As this is likely to occur also for α2 homomeric receptors, we recorded the macroscopic jumps using a low (10-mM) intracellular chloride concentration to make sure that in the different experiments, channels were exposed to similar chloride concentrations so that the information from different patch configurations could be combined in our investigation of the activation mechanism. Traces in Fig. 1 A are the outside-out current responses of α2 homomeric GlyRs to the fast application of 2-ms pulses of 10 mM glycine. The results of fitting the time course of current responses to short pulses of 0.5–10 mM glycine are shown in Table I. Two exponential components were needed to fit the current decay, and the slower component was the most prominent by far.

We also recorded outside-out α2 GlyR macroscopic responses to long (200-ms) concentration jumps at saturating glycine concentrations (10 mM; −100 mV; low [Cl⁻] pipette solution). A typical current example is shown in Fig. 1 B. All patches ($n = 6$) revealed a complex desensitization phase that could be best fitted with
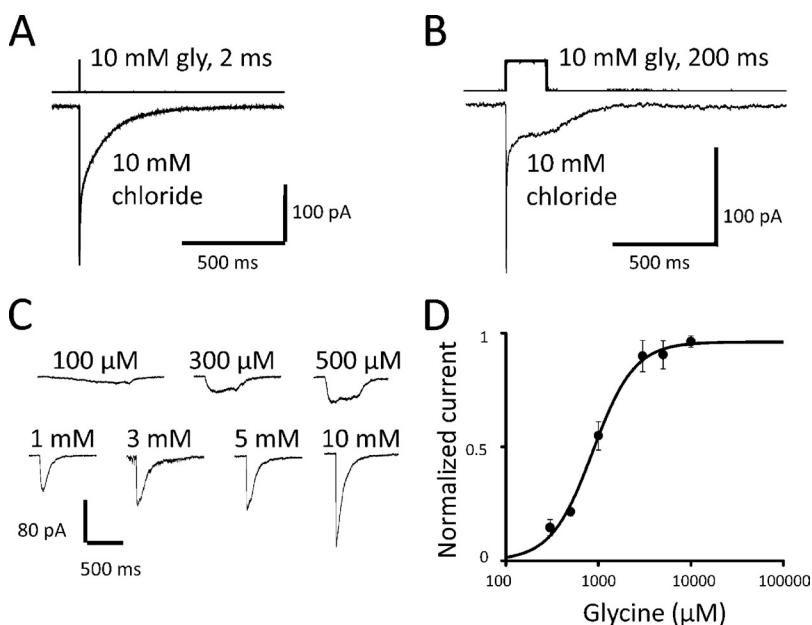
Figure 1. Macroscopic responses of α2 GlyR to rapid glycine application to outside-out patches. (A) The current trace represents the average of 12 sweeps evoked by a 2-ms concentration jump of 10 mM glycine applied to an outside-out patch (held at −100 mV) from a HEK293 cell expressing α2 GlyRs. Recordings were performed with 10 mM Cl⁻ pipette solution. The time course of glycine application, taken from the open tip response after seal rupture, is shown above the trace. (B) Similarly, the average current obtained with a long pulse (200 ms) of 10 mM glycine (average of 20 sweeps). Note the complex desensitization phase (for this patch the decay was fitted by three components, with time constants and areas of 1.8 ms, 0.5%; 25 ms, 1.5%; and 1,300 ms, 98%). (C) Traces are average currents elicited in one outside-out patch by two to five glycine applications using 10 mM Cl⁻ pipette solution. Glycine concentrations were applied in random order and for a time sufficient to obtain a peak current. (D) Concentration–response curve for glycine obtained from pooled data from outside-out currents as those in C (refer to Materials and methods for details). Currents were normalized to the fitted maximum for each experiment, and the pooled data were fitted with the Hill equation ($n = 6$).

mixtures of three exponential components: 1.9 ± 0.3 ms ($0.6 \pm 0.2\%$ fractional area), 23 ± 3 ms ($2.2 \pm 0.6\%$), and 820 ± 180 ms ($97.2 \pm 0.7\%$). This complexity of desensitization was independent of current amplitude: there was no apparent relationship between the peak current amplitude of the different patches and the number of the components needed for fitting currents.

Finally, to characterize the concentration–response relation for $\alpha2$ channels, we performed concentration jumps at a range of glycine concentrations. The traces in Fig. 1 C show examples of averaged currents recorded in the outside-out configuration using a low [Cl$^-$] pipette solution (10 mM chloride; -100 mV). Concentration–response curves obtained from six patches gave an average EC_{50} of 770 ± 100 µM and an n_H of 1.99 ± 0.25 (Fig. 1 D).

General features of $\alpha2$ GlyR single-channel activity

Fig. 2 A shows representative glycine-activated single-channel currents recorded in the cell-attached configuration (pipette holding potential of +100 mV) from HEK293 cells transfected with rat $\alpha2$ GlyR cDNA. It was immediately clear that the single-channel activity of $\alpha2$ GlyRs is very different from that of $\alpha1$ (Beato et al., 2004) or $\alpha1\beta$ GlyRs (Burzomato et al., 2004). Openings of $\alpha1$ or $\alpha1\beta$ GlyRs occur in short bursts at low glycine concentrations (Fig. 2 B, bottom trace). These bursts are activations that, as glycine concentration is increased, become more closely spaced because the time spent in unliganded resting states gets shorter until, in high glycine, they become grouped into long, high P_{open} clusters, separated by long shut periods.

In apparent contrast to what is seen with $\alpha1$ or $\alpha1\beta$ receptors, $\alpha2$ activity appeared to be very similar at all glycine concentrations (Fig. 2, A and B). Even at 20 µM, the lowest glycine concentration at which single-channel currents could be detected, groups of $\alpha2$ channel openings were long and separated by long shuttings (usually lasting for minutes). Because of the length of the shut times, each recording contained a relatively small number of these groups of openings and few long shut times.

Another consequence of the small number of long shut times that could be recorded is that it was impossible to measure any changes in their length as glycine concentration was increased. Moreover, the "experimental" success rate was generally low, and only a minority of $\alpha2$ patches displayed any channel activity ($\sim$1 in 5 patches at glycine concentrations of 100 µM or greater and only $\sim$1 in 10 at 20–50 µM). We could find no single-channel activity in records at 10 µM glycine, despite recording from >70 good patches for 5–25 min.

After idealization of single-channel records by time-course fitting, the distributions of apparent open and shut times were plotted and fitted with mixtures of exponential probability density functions. The distributions of apparent open periods are shown in Fig. 2 A (middle column). These were fitted with up to three exponential components (Table II). The longest component was predominant at all concentrations, with an average area of 82–98%, and had a time constant of $\sim$30 ms at all concentrations other than 20 µM glycine, where it appeared to be about threefold shorter. Both of the two faster components represent a very small number of intervals and were poorly defined, and a single-exponential density fitted the distribution quite well in most cases. The absolute number of apparent openings or shuttings per patch was small, despite the length of the clusters and the length of the recordings. Apparent shut-time distributions (Fig. 2 A, right column) were fitted with a minimum of three components (Table III). At all glycine concentrations, most shuttings were contributed by the shortest component (area, 85–99%). Given its average time constant of 5–10 µs, the vast majority of the events in this component were shorter than the experimental resolution of 20–25 µs and thus were missed. The number of shut-time intervals that fell into the two longest components was very small, and consequently, these components were not very well defined. The time constants of these two components appeared to decrease about threefold when glycine concentration increased from 20 µM to 10 mM. The existence of more than one shut-time component at saturating

TABLE I

Rise-time and decay-time constants of glycine concentration jump (2 ms) current responses

| [Glycine] (n)	Amplitude	Rise time 20–80%	Deactivation	
			$\tau1$ (fractional area)	$\tau2$ (fractional area)
mM	*pA*	*ms*	*ms*	*ms*
10 (13)	170 ± 30	0.42 ± 0.08	5.6 ± 0.8 ($3 \pm 3\%$)	130 ± 10 ($97 \pm 3\%$)
1 (13)	60 ± 10	1.1 ± 0.1	5 ± 2 ($1 \pm 2\%$)	92 ± 8 ($99 \pm 2\%$)
0.5 (9)	18 ± 4	1.2 ± 0.1	4 ± 1 ($1 \pm 1\%$)	83 ± 6 ($99 \pm 1\%$)

The deactivation phase was fitted with two exponential curves. Recordings were performed with low (10 mM) chloride in the pipette at -100 mV. Data are given as mean ± SDM.

concentrations (Fig. 2 A and Table III) is not compatible with mechanisms that have only one shut state when fully liganded. Additional fully bound shut states are therefore required, either as intermediates during channel opening or otherwise distal to the binding steps.

The records shown in Fig. 2 A show a superficial resemblance to the clusters of openings that are seen with other receptors at concentrations of agonist that are high enough to produce long desensitized intervals, but it seems that the appearance is deceptive. These long groups of openings appear to be unusually long individual activations of the channel, rather than clusters of many activations. This interpretation is confirmed by the analysis below.

The best way to display and characterize the concentration dependence of single-channel activity is to plot a one-channel concentration–P_{open} curve. This is done by identifying stretches of openings that are likely to be the expression of the activity of a single-channel molecule by setting for each idealized record a critical shut-time duration t_{crit} value (refer to Materials and methods). We attempted to construct a single-channel concentration–P_{open} curve for $\alpha 2$ receptors in this way, but it proved to be impossible. A typical display of the P_{open} values calculated for groups of openings, pooled and averaged, is shown in Fig. 2 C: the P_{open} was high, well above 90% at all agonist concentrations. Similar results were obtained at all the values of t_{crit} tested (1–100 ms). This is because (see Discussion) these groups represent channel activations, rather than clusters of several activations. Hence, the P_{open} data found in this way yielded no information about the concentration dependence of channel activity.
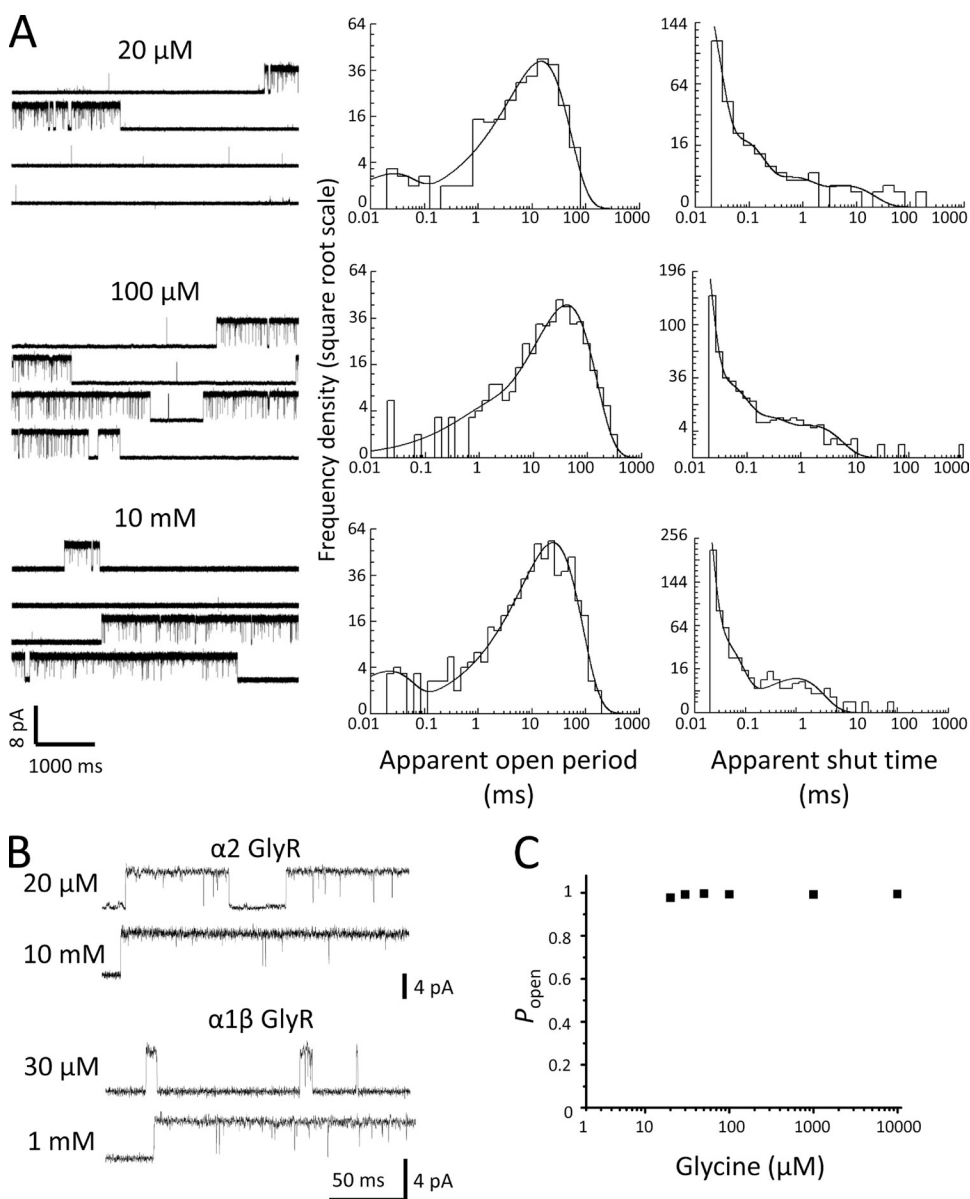
Figure 2. Single-channel properties of $\alpha 2$ GlyRs in the cell-attached configuration. (A) Traces on the left are continuous stretches (20 s) of single-channel currents from $\alpha 2$ GlyRs expressed in HEK293 cells (pipette holding V, +100 mV) recorded in the presence of 20 µM to 10 mM glycine (5–7-kHz filter). On the right are the corresponding open-period and shut-time distributions, fitted with mixtures of exponential probability density functions. (B) $\alpha 2$ GlyR single-channel currents in 20 µM and 10 mM glycine are compared with equivalent traces recorded from HEK293 cells expressing $\alpha 1\beta$ GlyRs, under similar recording conditions (from Burzomato et al., 2004). Note the long bursts for $\alpha 2$ channels at the low glycine concentrations. (C) The P_{open} concentration–response curve for $\alpha 2$ receptor clusters at a range of glycine concentrations is shown. Each point in the plot represents the average P_{open} value for all idealized patches at each concentration. The P_{open} for each patch was calculated as the ratio between the total open time and the total length of the clusters.

TABLE II

Empirical fit of mixtures of exponential probability density functions to the apparent open-period distributions

[Glycine]	τ1 Area (%)	τ2 Area (%)	τ3 Area (%)	Mean open time
	ms	*ms*	*ms*	*ms*
20 µM *n* = 2	0.017 ± 0.009 (15 ± 10)	0.20 (5)	13.1 ± 1.5 (83 ± 12)	12.5 ± 1.8
30 µM *n* = 2	0.011 ± 0.001 (12 ± 2)	0.52 ± 0.13 (5 ± 1)	37.4 ± 7.3 (82 ± 3)	34.4 ± 7.5
50 µM *n* = 2	0.051 (4)	—	29.0 ± 2.6 (98 ± 2)	28.7 ± 2.9
100 µM *n* = 3	0.029 (3)	0.562 ± 0.449 (4 ± 1)	31.0 ± 5.1 (97 ± 1)	30.1 ± 4.8
1 mM *n* = 3	0.023 ± 0.011 (11 ± 8)	—	30.4 ± 2.4 (93 ± 6)	29.9 ± 2.2
10 mM *n* = 3	0.018 ± 0.006 (4.33 ± 0.03)	—	34.8 ± 4.6 (97 ± 1)	32.9 ± 6.1

n is the number of idealized patches used for each concentration. The time constant value and fractional area (in brackets) of each component are the average ± SDM for each concentration.

Maximum likelihood fit of kinetic mechanisms: initial considerations

Next, we performed maximum likelihood fitting of kinetic mechanisms to our single-channel data, using HJCFIT. Single-channel records were grouped into sets, and each set contained four patches that spanned the range of glycine concentrations (refer to Materials and methods). Because (as above) we were not able to assess the concentration dependence of the single-channel P_{open} (e.g., Burzomato et al., 2004; Lape et al., 2008), for α2 receptors we had to rely on the macroscopic concentration–response curve (Fig. 1 D) for the choice of concentrations. Ideally, to provide sufficient information on the different steps of the mechanism, each set should include records from low, intermediate, and saturating concentrations of glycine.

Initial attempts to fit a range of concentrations up to 1 mM gave inconsistent results. However, the macroscopic concentration–response curve (Fig. 1 D) suggests that 1 mM glycine is not a saturating concentration. Much better results were obtained when single-channel recordings at 10 mM glycine were included in the fits. This inclusion of 10 mM of data was essential to obtain good agreement of the macroscopic deactivation time constant predicted by the fit with our measurements in the concentration jump experiments and to predict the distinctive, unusually long single-channel activations, separated by long shut times.

For fitting, the idealized records are divided into groups of openings that are separated by a shut time that is longer than a specified t_{crit}. The aim of this is to obtain groups of openings that come from the

TABLE III

*Empirical fit of mixtures of exponential probability density functions to the apparent shut-time distributions*

[Glycine]	τ1 Area (%)	τ2 Area (%)	τ3 Area (%)	τ4 Area (%)
	ms	*ms*	*ms*	*ms*
20 µM *n* = 2	0.010 ± 0.002 (89 ± 3)	0.092 ± 0.028 (8 ± 1)	0.589 ± 0.027 (3 ± 1)	6.06 ± 0.01 (1 ± 0.4)
30 µM *n* = 2	0.006 ± 0.001 (89 ± 2)	0.044 ± 0.014 (8 ± 2)	0.479 ± 0.055 (2 ± 0.2)	5.2 ± 2.5 (1 ± 0.2)
50 µM *n* = 2	0.005 ± 0.003 (99 ± 1)	0.085 ± 0.071 (0.9 ± 0.8)	—	2.83 (0.3)
100 µM *n* = 3	0.005 ± 0.001 (98 ± 1)	0.027 ± 0.007 (2 ± 1)	0.210 ± 0.042 (1 ± 0.3)	2.02 ± 0.66 (0.5 ± 0.2)
1 mM *n* = 3	0.007 ± 0.001 (92 ± 2)	0.045 ± 0.014 (6 ± 1)	0.354 ± 0.092 (2 ± 0.7)	1.97 ± 0.35 (0.9 ± 0.3)
10 mM *n* = 3	0.006 ± 0.001 (85 ± 12)	0.024 ± 0.005 (11 ± 9)	0.219 (6)	1.09 ± 0.05 (1.4 ± 1)

n is the number of idealized patches used for each concentration. The time constant value and fractional area (in brackets) of each component are the average ± SDM for each concentration.

same individual channel (refer to Materials and methods; Colquhoun et al., 1996, 2003). Because there was some ambiguity in the choice of t_{crit} (see about P_{open} curve above), we did several preliminary fits with different t_{crit} values. For most mechanisms tested, the fits were consistently more stable when the t_{crit} was set to 100 ms at 20–30 µM, 10 ms for bursts at higher concentrations (up to 1 mM), and 7–10 ms at 10 mM glycine.

To test the quality of a model, the predictions from a fit were compared with the experimental apparent shut-time and apparent open-period distributions. In this case, open and shut times were almost independent, so conditional distributions of open times were not a useful criterion for distinguishing mechanisms (Colquhoun and Hawkes, 1987; Colquhoun et al., 2003; Burzomato et al., 2004). Additional elements for evaluating the quality of a mechanism were the physical plausibility of the estimated rate constant values and their consistency across different sets. Finally, simulations of steady-state single-channel records and calculations of macroscopic currents (concentration jumps), on the basis of the model and rate constants that were fitted, were compared with our experimental data. In total, 44 different putative mechanisms were fitted (see Discussion). Most failed to describe
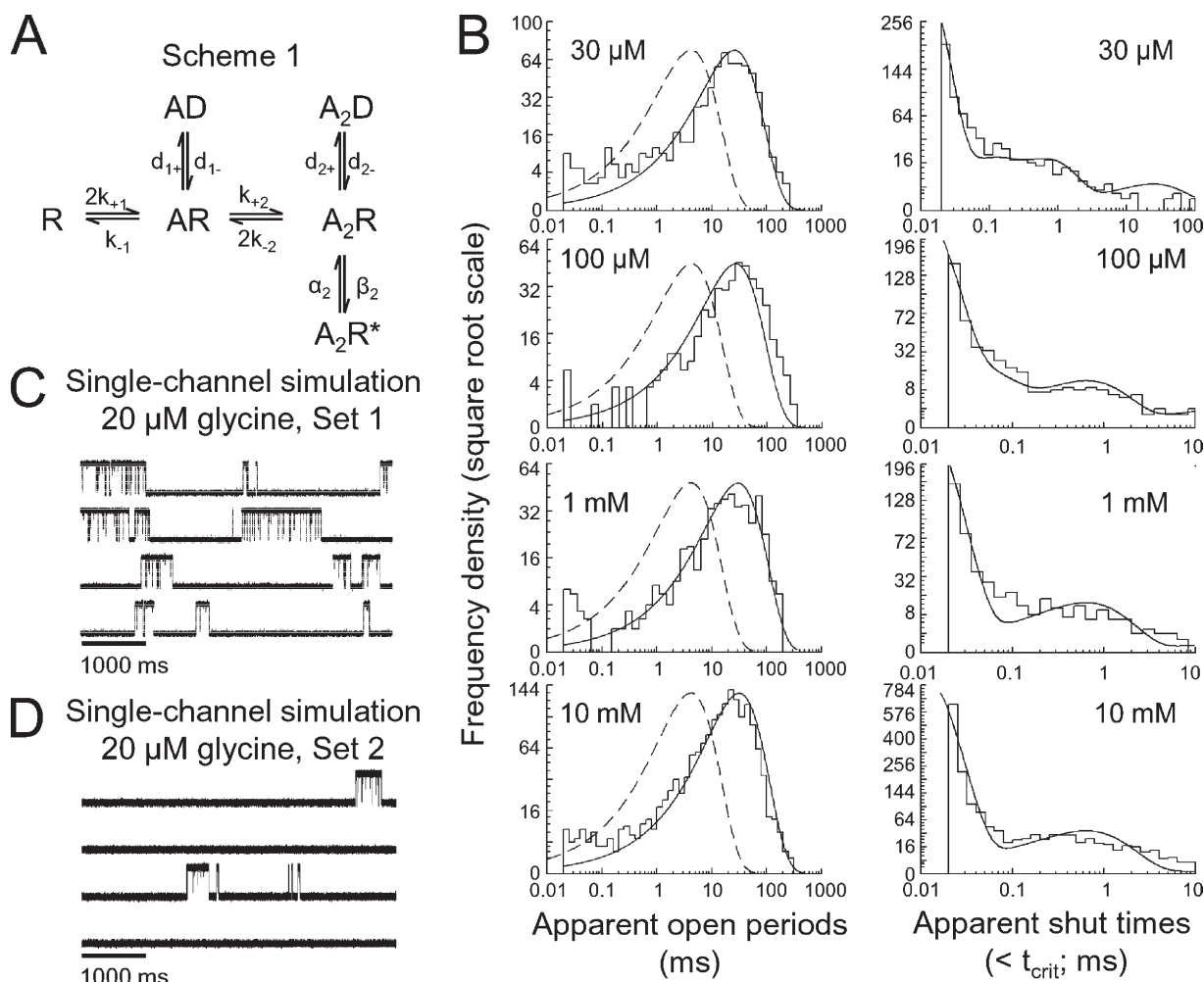
Figure 3. Fits of Scheme 1 to α2 single-channel data. (A) Scheme 1 (Mangin et al., 2003) contains two binding sites and a single open state linked to the fully liganded shut state. Directly connected to the bound shut states are short-lived desensitized states. Entry into these states is independent of glycine concentration. (B) The results of simultaneous fit of a dataset (containing four single-channel patches) with Scheme 1. The fit was performed with the assumption of interacting binding sites. The histograms are the experimental open-period and shut-time distributions, the continuous curves are the calculated distributions predicted from the model and fitted rate constants (resolution, 20 µs), and the dashed lines are the predicted fits at perfect resolution (i.e., when no events are missed). (C) Simulation of a single-channel record (at 20 µM glycine) using the fitted rate constants of one of the sets fitted with Scheme 1. This fit failed to predict the long shut times between groups of openings we observed in the experimental records, but it instead predicted that at low concentration we should observe frequent bursts. (D) Similar to C, using a different dataset (same set as in B), fitted with Scheme 1. Although this set can predict long gaps and clusters of openings, it also predicts very short bursts with lower P_{open} that are not observed at any of our single-channel records (compare with Fig. 2 A).

the data well, and only a few of the most plausible candidates will be described here.

Scheme 1: a mechanism with two binding sites and two extra shut states

Kinetic Scheme 1 (Fig. 3 A) has been proposed by Mangin et al. (2003) as a minimal kinetic mechanism for the $\alpha 2$ homomeric GlyR on the basis of the analysis of macroscopic and single-channel currents activated by fast agonist application to outside-out patches. Scheme 1 contains two short-lived "desensitized" states, each connected to a bound shut state. This scheme resembles closely the one proposed for the activation of GABA$_A$ receptors by Jones and Westbrook (1995). Good fits of apparent open periods and shut times could be obtained, but only if the binding sites were allowed to interact (i.e., no constraints imposed on the binding rates), as for the analogous model for $\alpha 1 \beta$ receptors (Burzomato et al., 2004).

Examples of distributions of apparent open periods and shut times for a set fitted with Scheme 1 are plotted in Fig. 3 B. As shown from this example, the fit of Scheme 1 predicts well the shape of the apparent shut- and open-time distributions. The results from the fits to three datasets are summarized in Table IV. As seen from the table,

TABLE IV

Estimated parameters from Scheme 1 fitted to $\alpha 2$ GlyR single-channel data

Parameter name and unit	Scheme 1
Rate constants ± CVM (%)	
α (s^{-1})	$330 \pm 17\%$
β (s^{-1})	$120{,}000 \pm 4\%$
d_{1+} (s^{-1})	$3{,}450 \pm 53\%$
d_{1-} (s^{-1})	$176 \pm 71\%$
d_{2+} (s^{-1})	$3{,}860 \pm 10\%$
d_{2-} (s^{-1})	$2{,}740 \pm 20\%$
k_{+1} (M^{-1}s^{-1})	$18{,}200 \pm 59\%$
k_{-1} (s^{-1})	$1{,}480 \pm 49\%$
k_{+2} (M^{-1}s^{-1})	$4.1 \times 10^8 \pm 75\%$
k_{-2} (s^{-1})	$6{,}680 \pm 49\%$
Equilibrium constants ± CVM (%)	
$E = \beta / \alpha$	$384 \pm 13\%$
$D_1 = d_{1+} / d_{1-}$	$28 \pm 63\%$
$D_2 = d_{2+} / d_{2-}$	$1.64 \pm 36\%$
$K_1 = k_{-1} / k_{+1}$ (μM)	$107 \pm 73\%$
$K_2 = k_{-2} / k_{+2}$ (μM)	$571 \pm 97\%$
P_{open} curve parameters (±SDM) predicted from this scheme	
max P_{open}	0.995 ± 0.001
EC_{50} (μM)	134 ± 55
n_{H}	1.94 ± 0.03

Rate constants are means of fits to three data sets ± CVM. The equilibrium constants (E, D_1, D_2, K_1, and K_2) are the means of the three values calculated for each separate set. Also listed are the average max P_{open}, EC_{50}, and Hill slope calculated from the fitted rate constants (±SDM). These fits have 10 free parameters.

the values for the gating rate constants (the shutting rate constant α and the opening rate constant β) were highly consistent across the three sets, with a very low coefficient of variation.

Rate constants other than those for opening and shutting were highly variable across the three sets (coefficient of variation [CVM] of 50% or more), suggesting that the scheme cannot estimate these rate constants reliably. Note also that the EC_{50} predicted from the fitted rate constants was almost sixfold lower than the EC_{50} measured in outside-out recordings. To test further the correctness of Scheme 1, we calculated the macroscopic current expected in response to 2-ms fast concentration jumps with 10 mM glycine. The current response was calculated for each set of fitted rate constants. The predicted rise time of macroscopic currents from the three sets fitted had a mean time constant of 10 ± 5 ms, which is $\sim$25-fold slower than the 20–80% rise time measured from currents evoked by 10 mM glycine ($\tau = 0.42 \pm 0.08$ ms; Table I). On the other hand, the mean deactivation time constant predicted by Scheme 1 was 120 ± 70 ms ($n = 3$ sets), which is very close to the experimental value of 130 ± 10 ms (the slow component; Table I). This corresponds to a mean burst length calculated from Scheme 1 of 120 ± 70 ms at 1 nM glycine ($n = 3$ sets).

We also checked whether simulated single-channel records (SCSIM program) resembled the pattern seen in experimental records. Single-channel simulations at 20 μM glycine using Scheme 1 failed to reproduce the most striking features we observed in our single-channel experimental records, namely the presence of groups of openings with duration of up to a few seconds long, separated by very long gaps lasting for minutes. For two sets, bursts (with lengths ranging from tens of milliseconds to $\sim$1 s) appeared continuously in the simulated records, and there was no sign of the very long shut times between them, as seen in experimental records (compare Fig. 3 C with Fig. 2 A). Only the simulation from the third set showed long gaps (Fig. 3 D), but even this realization did not show long, high P_{open} groups of openings. The mean burst length calculated from Scheme 1 at 20 μM glycine was only 300 ± 30 ms ($n = 3$ sets). These simulations show that Scheme 1 could not describe our experimental results adequately, despite a good match to the dwell-time distributions. Therefore, we proceeded to test alternative mechanisms for our data.

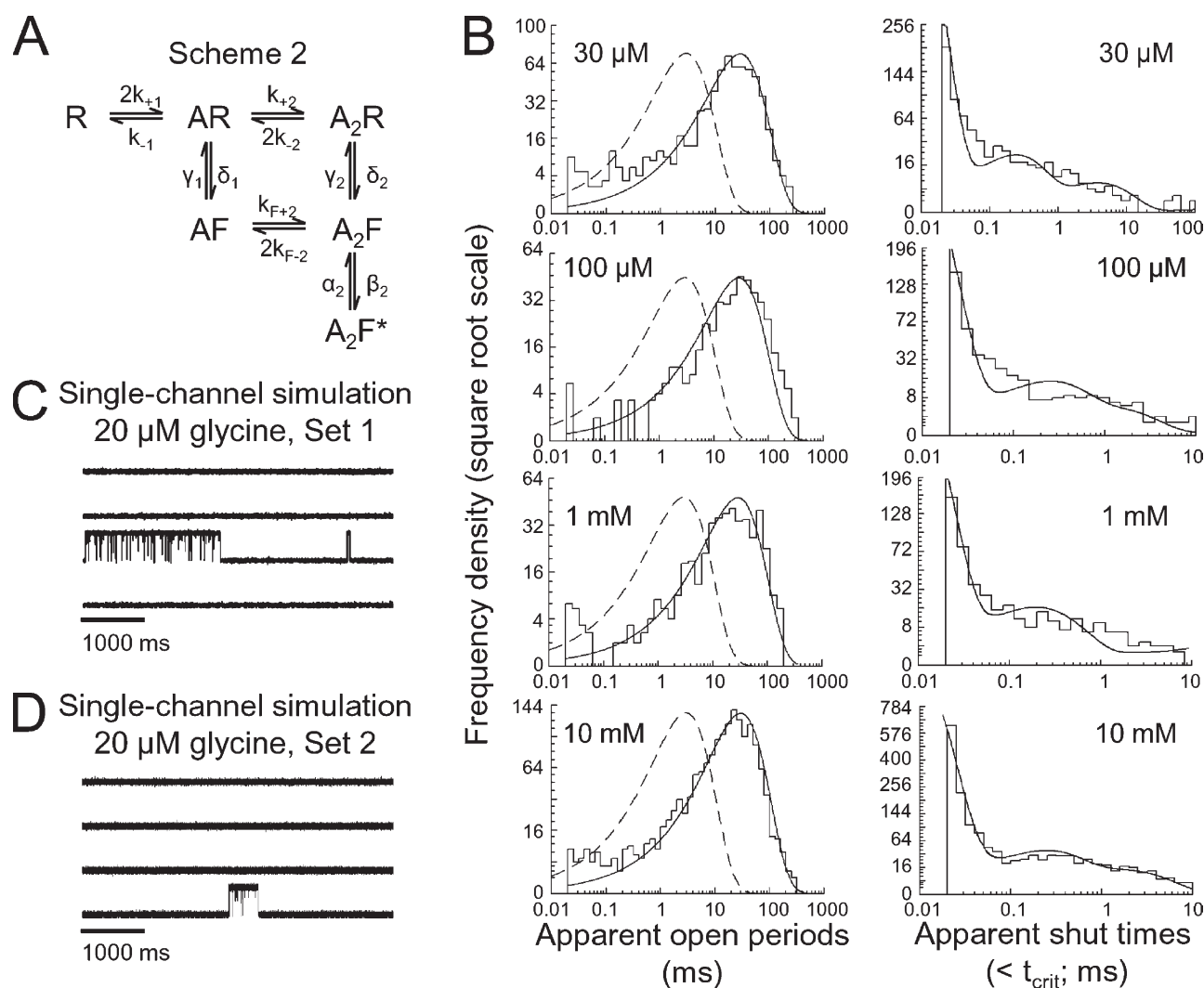## Scheme 2: a flip mechanism with two binding sites and one open state

Kinetic Scheme 2 (Fig. 4 A) is a variant of the flip mechanism, originally proposed by Burzomato et al. (2004) for $\alpha 1 \beta$ and $\alpha 1$ GlyRs. Scheme 2 is a modified version containing two binding sites (rather than the three needed to reach maximum P_{open} in $\alpha 1$ homomers). We have also chosen to omit from Scheme 2 the two partially liganded open states included in the $\alpha 1 / \alpha 1 \beta$ flip mechanism.

Including more than one open state in the mechanism barely improved the quality of the fits to the present data and resulted in poorly determined rate constant estimates for the entry and exit from partially liganded open states. This probably means that openings from partially liganded receptors are rare, so there are not enough transitions in our records to be able to describe these states accurately. The predominance of visits to a single open state is confirmed by the lack of any substantial correlation between open and shut times, and by the fact that the distribution of apparent open-period durations is not far from a single exponential.

An example of a dataset fit with Scheme 2 is shown in Fig. 4 B. There is a good agreement between the experimental distributions (histograms) and those that are

predicted from the fits using the model (continuous line). The set shown in Fig. 4 B is the same as in Fig. 3 B for comparison. The average rate constants from three different sets are summarized in Table V. Note that these fits were done with the assumption that binding sites are independent; i.e., they do not interact, so all binding steps to a given conformation (R or F) are identical, regardless of how many sites are already occupied. This was done by imposing the constraint that $k_{+1} = k_{+2}$ and $k_{-1} = k_{-2}$.

As seen from the values in Table V, the fits with Scheme 2 are very consistent across the three sets, and most rate constants had low coefficients of variation. The least well-defined rate constants are those for entering and exiting the singly occupied flip state (δ_1 and γ_1),

Figure 4. Fits with a flip model containing two binding sites (Scheme 2). (A) Scheme 2 is a flip model with two binding sites and a single open state that can be accessed from the fully liganded shut state after flipping. (B) Plots that show open-period and shut-time distributions fitted with Scheme 2. The same set of four patches is used as in Fig. 3 B for comparison. The fits with Scheme 2 are performed using constraints for non-interacting binding sites (resolution, 20 μs). (C and D) Simulation of a single-channel record (at 20 μM glycine) using the fitted rate constants of two of the sets fitted with Scheme 2 (the set in D is the one shown in the histograms). The predictions from all sets fitted with this model are in a very good agreement with the observed single-channel records (compare with Fig. 2 A).

although they are clearly quite slow. This is not surprising given the evidence already cited that partially liganded states occur only rarely. Scheme 2 again predicts that the efficacy for the opening step is very high (350), and that the efficacy for the flipping steps increases as the number of bound glycine molecules increases (Table V). Also, the shut flipped states have a 40–60-fold higher affinity for glycine than the shut resting states. This is a well-characterized feature of the flip mechanism, which suggests that the binding of the agonist stabilizes the receptor in a higher affinity form reached by a conformational change that precedes channel opening (Burzomato et al., 2004). The average maximum P_{open} predicted by the fits to Scheme 2 was 0.99, and the predicted n_H was 1.89, in good agreement with the value of 1.99 (n_H; Fig. 1 D) obtained from our macroscopic dose–response curve experiments (see also Mangin et al., 2003) and with the maximum P_{open} of 0.99 from single-channel records. Note, however, that there was about a threefold difference between the experimental macroscopic EC_{50} (770 µM) and the one predicted by the model (240 µM; Table V).

Using the rate constants obtained from the fits described above, we calculated macroscopic current responses to a 2-ms fast concentration jump with 10 mM glycine. Scheme 2 predicted a time constant of 171 ± 6 ms (n = 3 sets) for the decay of these currents, which is similar to the 130 ± 10 ms we obtained from our macroscopic currents in outside-out patches. Scheme 2 predicted two significant components for the activation phase of the current macroscopic current (1.6 ± 0.2 and 0.19 ± 0.02 ms), but the contribution of the faster component was minimal. Consequently, the weighted calculated rise time (τ = 1.5 ± 0.2 ms) reflected mostly the slow component and was almost fourfold slower than the rise time measured from currents evoked by 10 mM glycine (20–80% rise time, 0.42 ± 0.08 ms; Table I).

Finally, steady-state single-channel records (at 20 µM glycine) simulated using the fitted rate constants showed groups of openings with a mean burst length of 490 ± 70 ms, separated by long shut times (>1 min; Fig. 4, C and D). These features of single channels are similar to our cell-attached recordings. It is not surprising that we

TABLE V

Estimated parameters from Schemes 2, 3a, and 3b fitted to α2 GlyR single-channel data

Parameter name and unit	Scheme 2	Scheme 3a	Scheme 3b
Rate constants ± CVM (%)			
α (s^{-1})	366 ± 12%	320 ± 3%	321 ± 4%
β (s^{-1})	127,000 ± 9%	119,919 ± 7%	120,000 ± 8%
γ_1 (s^{-1})	4 ± 81%	292 ± 98%	–
δ_1 (s^{-1})	0.134 ± 76%	0.014 ± 82%	–
γ_2 (s^{-1})	4,418 ± 11%	2.1×10^{-7} ± 48%	106 ± 100%
δ_2 (s^{-1})	4,316 ± 12%	1.7×10^{-9} ± 42%	0.36 ± 100%
γ_3 (s^{-1})	–	4,109 ± 20%	4,152 ± 19%
δ_3 (s^{-1})	–	2,572 ± 38%	2,605 ± 38%
k_{F+} (M^{-1}s^{-1})	7.9×10^6 ± 27%	3.1×10^7 ± 61%	2.4×10^7 ± 75%
k_{F-} (s^{-1})	677 ± 12%	719 ± 37%	659 ± 42%
k_+ (M^{-1}s^{-1})	1.04×10^5 ± 5%	0.779×10^5 ± 21%	0.781×10^5 ± 26%
k_- (s^{-1})	439 ± 22%	154 ± 36%	158 ± 38%
Equilibrium constants ± CVM (%)			
$E = \beta/\alpha$	347 ± 6%	373 ± 4%	372 ± 4%
$F_1 = \delta_1/\gamma_1$	0.031 ± 28%	2.2×10^{-4} ± 63%	–
$F_2 = \delta_2/\gamma_2$	0.977 ± 24%	0.011 ± 47%	0.017 ± 52%
$F_3 = \delta_3/\gamma_3$	–	0.573 ± 31%	0.570 ± 29%
$K_R = k_-/k_+$ (µM)	4,241 ± 26%	1,879 ± 21%	1,919 ± 20%
$K_F = k_{F-}/k_{F+}$ (µM)	86 ± 37%	31 ± 21%	48 ± 29%
$K_R/K_F = F_2/F_1$	46.5 ± 28%		
Predicted P_{open} curve parameters ± SDM			
max P_{open}	0.990 ± 0.006	0.993 ± 0.002	0.993 ± 0.002
EC_{50} (µM)	243 ± 52	389 ± 66	400 ± 67
n_H	1.89 ± 0.005	2.49 ± 0.06	2.49 ± 0.05

Rate constants are means of fits to three data sets ± CVM. The equilibrium constants (E, F_1, F_2, F_3, K_R, and K_F) are calculated for each separate fit, and means are listed here (because of the variability, the means of the equilibrium constants are not exactly the same as the ratios of the mean rate constants). Likewise, the mean values of the relative affinity of glycine for resting and flipped (K_R/K_F) are given. Also listed are the average max P_{open}, EC_{50}, and Hill slope calculated from the fitted rate constants (±SDM). The number of free parameters: 9 out of 12 in Scheme 2, 10 out of 18 in Scheme 3a, and 9 out of 14 in Scheme 3b. Other rate constants are set by microscopic reversibility or constrained by the assumption that the binding sites are equivalent and independent.

saw no channel activity at 10 µM glycine, because calculations based on the fitted rate constants predict that activations should be separated by long silent periods of >4 min (see Discussion).

To summarize, based on the above observations and on preliminary fits to different models, Scheme 2 is the minimal model that can describe best both our single-channel and macroscopic data.

Scheme 3: a flip mechanism with three binding sites and one open state

The mechanism in Scheme 2 contains two binding sites. This is different from what we suggested earlier for the α1 homomeric GlyR, namely that maximal activation of the receptor requires the occupancy of three binding sites by glycine (Beato et al., 2004). It is of course possible that the number of functional binding sites is different between α2 and α1 homomers, but this is an important point to test. We therefore extended Scheme 2 and tested two related mechanisms (Scheme 3a and Scheme 3b), shown in Fig. 5 A. The two mechanisms differ only in that the monoliganded flipped state AF is omitted from Scheme 3b. As for Scheme 2, we assumed that binding sites are identical (within each form of the receptor) and do not interact. This was imposed by using the following constraints: $k_{+1} = k_{+2} = k_{+3}$ and $k_{-1} = k_{-2} = k_{-3}$ for both R and F states. Note that because of these constraints, the number of free parameters in Schemes 2 and 3b is the same, and both have nine free rate constants.
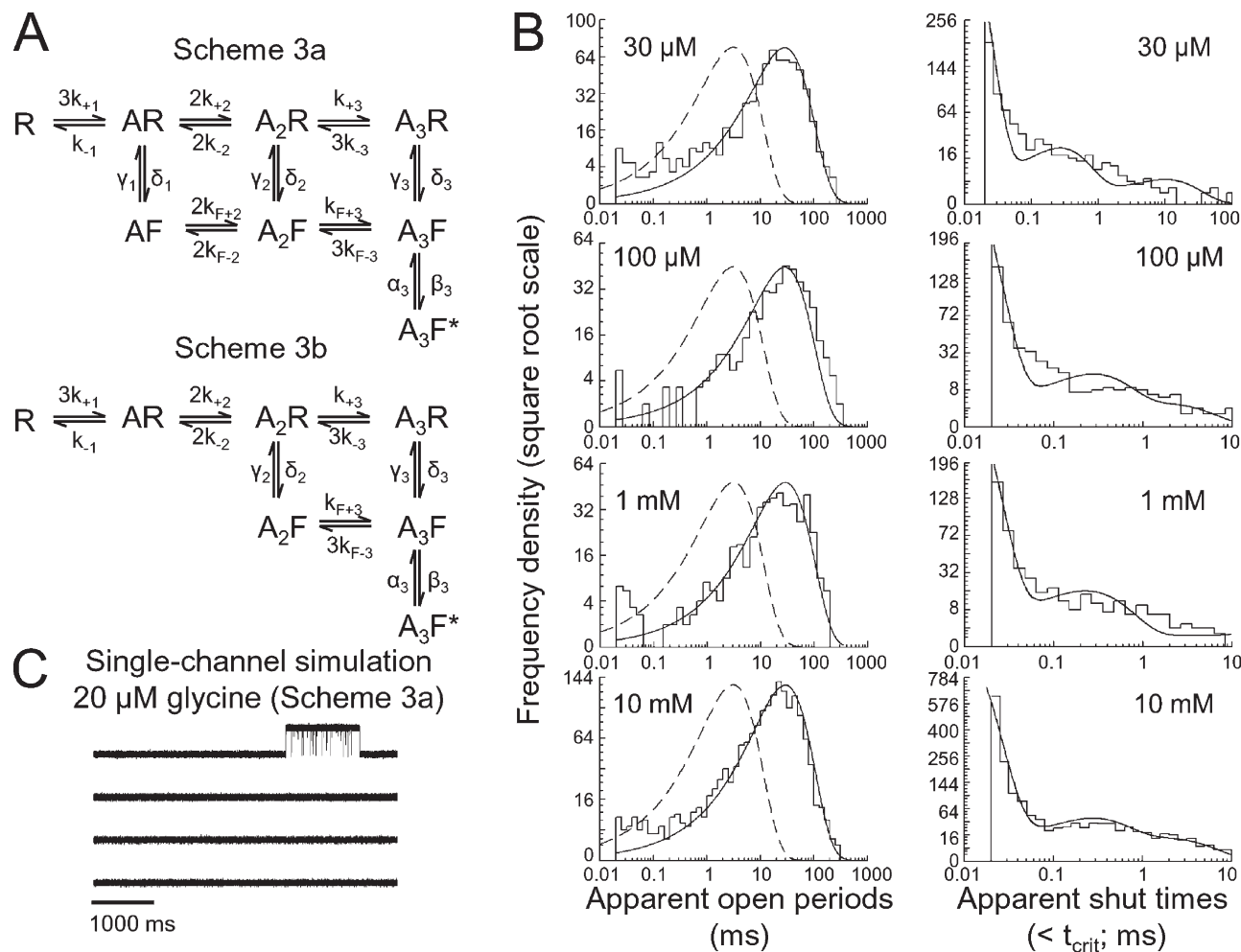
Figure 5. Fits with flip models containing three binding sites (Schemes 3a and 3b). (A) Scheme 3a (top) differs from Scheme 2 (Fig. 4 A) in the presence of a third agonist binding site. Scheme 3b (bottom) is a variant that lacks the partially liganded AF state. Both models have only one open state that can be accessed after flipping, when the three binding sites are occupied by glycine. (B) Plots that show open-period and shut-time distributions fitted with Scheme 3a. Identical fits were obtained with Scheme 3b. Note also the similarity with predictions from Scheme 2 (Fig. 4 B). Fits with models 3a and 3b were performed with constraints for non-interacting binding sites (resolution, 20 µs). (C) Simulation of a single-channel record (at 20 µM glycine) using the fitted rate constants of the set shown in B. Similar simulations are obtained for Scheme 3b. The prediction from both models is similar to those from Scheme 2 and in a very good agreement with our cell-attached data (compare with Figs. 2 A and 4, C and D).

The apparent quality of the predictions of the dwell-time distributions was good and very similar for the two models; therefore, we show only the fits of Scheme 3a in Fig. 5 B, using the same set of data as in the previous figures for comparison. The predictions of the dwell-time distributions were almost identical for Schemes 2, 3a, and 3b (compare Fig. 4 B and 5 B), and the values of the rate constants obtained by fitting the three schemes (see Table V) were very similar, although the coefficient of variation was overall higher for the fits with Scheme 3b. The most variable rate constants are again those that describe the transitions between partially liganded flipped and resting states.

Scheme 2 is favored over Schemes 3a and 3b because of its better prediction of the Hill slope (1.89 ± 0.01 for Scheme 2, but 2.49 ± 0.06 for Scheme 3a and 2.49 ± 0.05 for Scheme 3b; see also Table V). Because we were not able to obtain a one-channel P_{open} curve, our only experimental estimate of a slope ($n_H = 1.99$; Fig. 1 D) comes from the concentration–response curve obtained from the macroscopic current records in the outside-out configuration. We do not know how much this measurement is distorted by desensitization, so this is not a conclusive argument.

To check further the quality of Schemes 3a and 3b, we calculated macroscopic currents and simulated single-channel currents. Fig. 5 C shows a simulated single-channel trace (20 µM glycine), using the rate constants from a set fitted with Scheme 3a. In this record, openings occur in groups several hundred milliseconds long, separated by very long shut times, as in our experimental traces. Similar results were obtained from simulations with Scheme 3b (not depicted). Therefore, as with Scheme 2, Schemes 3a and 3b predicted well our single-channel data. The rise and deactivation time constants of macroscopic currents were calculated from the fitted rate constants. The average weighted rise time of a calculated current activated by 2 ms of 10 mM glycine was 1.5 ± 0.4 ms ($n = 3$ sets), and the deactivation time constant was 150 ± 30 ms. Both time constants were almost indistinguishable from those calculated for Scheme 2. The relationship between burst length and macroscopic deactivation is considered in the Discussion.

DISCUSSION

The main aim of this paper is to characterize the activation mechanism of homomeric α2 GlyRs. We used the method of maximum likelihood fitting of kinetic mechanisms to idealized single-channel data (Colquhoun et al., 2003) for the α2 GlyR. In brief: (a) single-channel data are idealized by time-course fitting, and patches of different agonist concentrations are grouped into sets; (b) a kinetic mechanism is postulated (usually taking into account exponential fits to experimental dwell-time distributions) and initial guesses are given for the rate constants; (c) the idealized records, the appropriate resolution, and the postulated mechanism are introduced into a program (HJCFIT) that can calculate the likelihood (i.e., the probability of the entire sequence of apparent open and shut times, given the current estimates of the rate constants) and maximize it by optimizing rate constants; and finally, (d) the validity of the model and of the final rate constants is checked by comparing their predictions with the experimental data (dwell-time histograms). For the α2 GlyR, we also examined how well the mechanism and rates fitted to single channels predicted the time course and concentration dependence of the macroscopic currents elicited by concentration jumps. The terms activation, burst, and cluster are defined at the beginning of the Results section.

Properties of α2 GlyR single-channel activity

The first kinetic analysis on GlyRs, performed on cultures of spinal motorneurons, showed a characteristic feature of these channels: the frequency of long and short openings is concentration dependent. In recordings at low glycine, increasing glycine concentration increases the proportion of long openings (without changing the time constants of the different opening components; Twyman and Macdonald, 1991). The same phenomenon was subsequently detected in recombinant homomeric and heteromeric GlyRs that contain the α1 subunit, where bursts at higher glycine concentrations are longer because they contain more openings and because the openings themselves appear to be longer (Fucile et al., 1999; Beato et al., 2002, 2004; Burzomato et al., 2004).

This is not the case for the activity of α2 GlyRs, where openings occur in long groups, regardless of concentration (Fig. 2 A). At first, the length of the groups of openings (Fig. 2 A) misled us into thinking that they were clusters (as defined above). Even at the lowest concentration of glycine at which channel activity could be obtained (20 µM), long groups of openings were observed (several hundreds of milliseconds), and the probability of being open within the group of openings was high (0.96; t_{crit}, 100 ms). However, the macroscopic concentration–response curve (Fig. 1 D) suggests that 20 µM glycine should produce only a very small response and therefore a very low overall single-channel P_{open} (<5%). This observation, together with the fact that we could not observe activity at concentrations lower than 20 µM, implies that the long groups of openings at 20 µM glycine must be (unusually long) individual activations of the channel (possibly lengthened a bit by rebinding). In other words, the true P_{open} must be low at 20 µM and should be measured including the very long shut periods that separate the groups of openings. This cannot be done because there is no way to tell whether two adjacent activations originate from the same individual channel.

The use of concentration jumps for fast agonist application provides the benefit of mimicking what occurs in vivo: a fast and brief exposure of the receptors to saturating concentrations of neurotransmitter in the cleft during synaptic transmission (Clements et al., 1992; Colquhoun et al., 1992). Moreover, when the application of agonist is short (1–2 ms), the decay of the current is known to reflect the duration of the burst at very low agonist concentration, i.e., the duration of channel activations (Wyllie et al., 1998). When jumps of 2 ms to three different glycine concentrations were applied, two deactivation components were identified. The time constant of the slow component, which is by far the predominant one, was ~130 ms, which is ~17 times slower than the deactivation of $\alpha 1\beta$ channels (7.5 ms with 10 mM intracellular Cl^-; Pitt et al., 2008). Note that Mangin et al. (2003) reported for $\alpha 2$ currents, using high chloride in the pipette, a deactivation time course similar to the one we observed (153 ms). We found (unpublished data) that changing intracellular chloride concentration to 130 mM had little effect on $\alpha 2$ currents, in contrast with our findings for $\alpha 1\beta$.

Choice of mechanism

Despite the fact that the single-channel records look very different from those seen with $\alpha 1$-containing homomers or heteromers, it was found eventually that the best description among the 44 mechanisms that we tested was provided by the flip model (Burzomato et al., 2004; Lape et al., 2008). An overview of the type of mechanisms tested is shown in Fig. 6.

The fit of the shut-time distributions was not perfect with this mechanism, and neither was the prediction of the rise time for concentration jumps. However, both were better than could be obtained with the main rival class of mechanisms, as represented here by the Mangin/Jones-Westbrook type of model (Scheme 1). In our original work on the flip model (Burzomato et al., 2004), the Jones-Westbrook–type mechanism fitted at least as well as flip, albeit with four more free parameters. The preference for the flip model then was based to a certain extent on physical grounds (it allowed a fit without having to postulate interaction between different binding sites), partly because the flip model had a plausible structural interpretation (C-loop capping, since confirmed in muscle nicotinic channels by Mukhtasimova et al., 2009). Mechanisms with preopening intermediate states work well for wild-type and mutant GlyR and muscle nicotinic channels and for $GABA_A$ channels (Burzomato et al., 2004; Plested et al., 2007; Lape et al., 2008; Mukhtasimova et al., 2009; Keramidas and Harrison, 2010). In the present case, there was more reason to discard a Mangin/Jones-Westbrook type of model in favor of flip than in our earlier work. For example, the fits with flip give more consistent rate constant values across experimental sets. Flip is also somewhat better at predicting EC_{50} values, the rise time of macroscopic currents, and the pattern of channel activity in single-channel records.

There are two respects in which the fit with the flip mechanism (Scheme 2), despite being the best we found, is less than perfect. The EC_{50} predicted by the fit to Scheme 2 was almost three times smaller than that observed for the macroscopic concentration–response curve. Also, the predicted rise time for responses to pulses of 10 mM glycine was over three times slower than the observed value (although that is a great deal closer than for Scheme 1, for which it was 25 times too slow). It could well be that the flip model is too simple to account for these details. The least plausible aspect of the flip mechanism is the postulate that flipping is a concerted conformation change. It might be better to allow flipping (or "priming") to occur separately in each subunit (Mukhtasimova et al., 2009). Desirable though that might be, in its general form, the primed model has so many free parameters that they cannot all be estimated from the data. We have preferred an approximation that allows all of the rate constants to be estimated.

Features of the activation mechanism for $\alpha 2$ GlyRs: the number of open states and binding sites

The general flip model that describes the activation of homomeric $\alpha 1$ and heteromeric $\alpha 1\beta$ GlyRs contains three open states (Burzomato et al., 2004). This is in line with early data on native and recombinant receptors that detected at least three distinguishable open states (Twyman and Macdonald, 1991; Beato et al., 2002, 2004; Lewis et al., 2003). In contrast to the $\alpha 1$-containing channels, $\alpha 2$ receptors could be fitted quite well with a flip model that contains only one open state. This suggests that partially liganded openings are either rare or too short to be detected. The latter explanation is supported by preliminary fits with a version of Scheme 2 that included monoliganded openings (not depicted). Partially liganded openings had a very high closing rate constant and were so short that, if they truly occurred, most of them would be missed with our resolution of 20 or 25 μs. For these reasons, we considered it more sensible to leave only one fully liganded open state. Another reason for this choice is that we could not detect open–shut correlations in our experiments with $\alpha 2$ receptors, and these are not expected to occur in mechanisms with only one open state (Colquhoun and Hawkes, 1987).

In the general flip scheme used to fit homomeric $\alpha 1$ channels, maximum P_{open} is reached when three (out of the possible five) binding sites are occupied by glycine. For the $\alpha 2$ channel, good, almost identical fits of single-channel data were obtained with flip mechanisms with two or three binding sites, and these

resulted in very similar values for the rate constants. The biggest difference between the predictions of mechanisms with two or three binding sites was in the value of the Hill slope of the concentration–response curve. Scheme 2 (two binding sites) predicted a value of 1.9, in better agreement with our experimental data from macroscopic currents in the outside-out configuration (1.99; Fig. 1 D). The limitation is that we only have a macroscopic concentration–response curve, which is less satisfactory than a single-channel P_{open} curve because it is susceptible to errors from desensitization, as well as possible differences between outside-out patches and cell-attached patches. Even so, it is clear that occupancy of all the five potential agonist binding sites in a homomeric nicotinic-type receptor is not needed to achieve the maximum P_{open}, in agreement with our own conclusions for the α1 GlyR homomer (Beato et al., 2004) and with those of the elegant experiments of Rayes et al. (2009) on α7-5HT$_3$ chimeric receptors.

Features of the activation mechanism of α2 GlyRs: efficacy and affinity

For the purpose of characterizing the kinetic behavior of homomeric α2 GlyRs, steady-state single-channel data were fitted to 44 different putative reaction schemes, only four of which are described here. These potential mechanisms fall into two distinct types. In Scheme 1, originally proposed by Mangin et al. (2003), the saturated receptor has only two states, open and shut, and the efficacy of the agonist depends only on the equilibrium constant for this step, $E = \beta_2/\alpha_2$, in the classical way. The maximum P_{open} is

$$P_{open}(\text{max}) = \frac{E}{1+E}. \tag{1}$$

To get good fits, it was necessary to add two extra shut states, in the manner of Jones and Westbrook (1995). Although these states are labeled as "desensitized," they are quite short-lived, and there is no reason to think
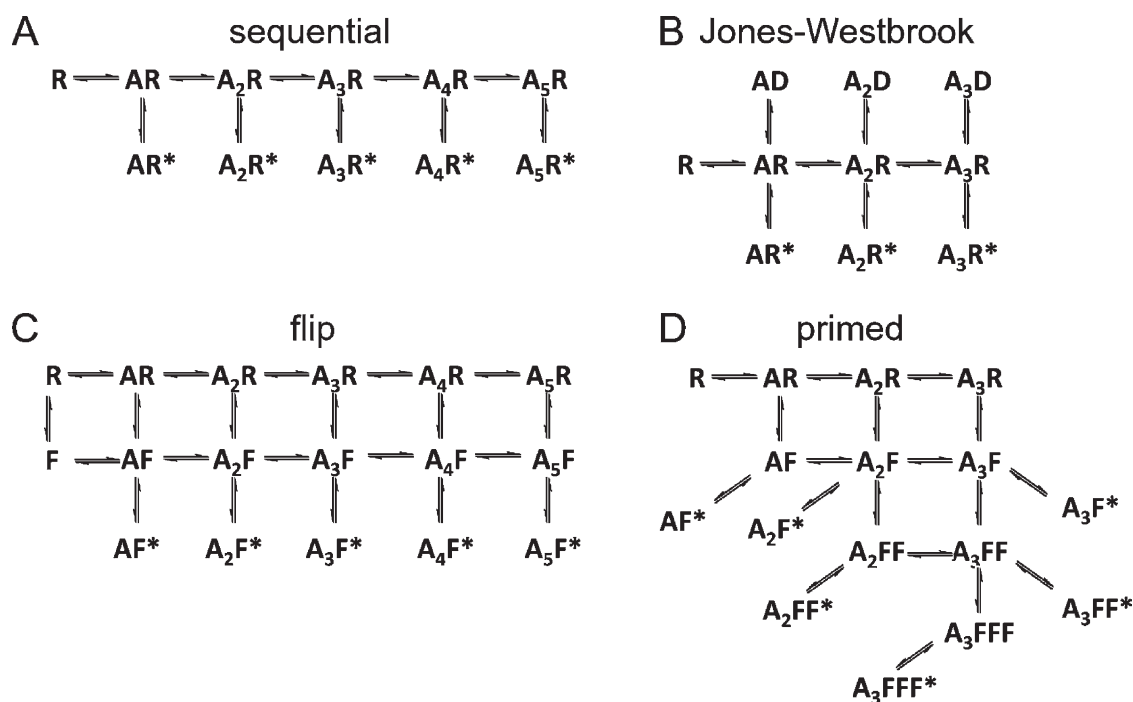
Figure 6. Activation mechanisms tested by global fitting to single-channel data. The mechanisms shown here are the most general forms of each of the 44 mechanisms we tested. In all schemes, the letter A denotes an agonist molecule and its subscript indicates the number of agonist molecules bound to the receptor. The letters R and R* denote resting shut states and open states of the receptor, respectively. (A) Sequential scheme with five binding steps and open states (nine "subset" schemes tested in all, with two to five binding steps, allowing opening either from each bound state or only from the one or two highest liganded states). (B) Jones and Westbrook–type scheme (Jones and Westbrook, 1995), with an open state and a distal desensitized state (indicated by D) for each binding step (five schemes tested with one to three binding steps, each leading to a desensitized state, allowing the channel to open only from the highest liganded states). (C) Flip-type scheme, where an intermediate flipped shut state (F) connects resting and open states (Burzomato et al., 2004; five schemes tested with one to five binding steps, a single flipped state, and a single open state; eight schemes tested, where the number of flipped and open states was either the same as the number of binding steps or smaller; three schemes tested, where, after the first binding step, the agonist can bind only to flipped states; three schemes with additional flipped states). (D) A subset of the primed mechanism (generalization of the flipped mechanism [Mukhtasimova et al., 2009]; 11 schemes tested with two to three binding steps and fewer open states than the maximum shown here). Several independent priming steps can occur. Here, the channel can open after one, two, or three priming steps (indicated as F, FF, or FFF).

that they have anything to do with macroscopic desensitization. The extra shut states are, therefore, entirely arbitrary. Furthermore, to obtain a good fit, it was necessary to assume that the two binding sites in Scheme 1 interact (the binding constant for the second binding is not the same as for the first).

For both of these reasons, we turned to flip mechanisms (Schemes 2, 3a, and 3b). In this class of mechanisms, the binding sites are supposed to be independent, and there is an extra shut state (the flipped conformation) between resting and open states. Therefore, the fully saturated receptor has three states (resting, flipped, and open) rather than two, and the maximum P_{open} depends on two different equilibrium constants. These are the equilibrium constant, E, for the open–shut reaction of the fully liganded receptor (the "opening efficacy"), and the equilibrium constant for the preceding conformation change from resting to flipped state, F (the "flipping efficacy"),

$$P_{open}(max) = \frac{EF}{1 + F(1 + E)}. \quad (2)$$

This can be written in the classical form if we define an "effective efficacy," E_{eff}, as

$$E_{eff} = E\frac{F}{1 + F}. \quad (3)$$

With this definition, the maximum P_{open} for the flip type mechanism can be written in the form of Eq. 1 as:

$$P_{open}(max) = \frac{E_{eff}}{1 + E_{eff}}. \quad (4)$$

The flip mechanism was first proposed for glycine $\alpha1\beta$ receptors by Burzomato et al. (2004). It follows from Eq. 3 that if the flipping efficacy, F, is small, the overall efficacy may be much lower than expected from the opening efficacy, E, and Lape et al. (2008) gave evidence that a reluctance to flip (small value of F) was the basis of partial agonism for both glycine and nicotinic receptors. A similar explanation for the partial agonism of choline at nicotinic receptors was proposed by Lape et al. (2009).

The fits of the flip mechanism (Scheme 2) suggested that glycine has a 46-fold higher affinity for the flipped conformation than for the resting conformation, little different from the 65-fold higher affinity for $\alpha1\beta$ GlyRs found by Burzomato et al. (2004). The results resemble $\alpha1\beta$ GlyRs also in that the increase in affinity is brought about almost entirely by an increase in the association rate constant for the flipped conformation, rather than a decrease in the dissociation rate. The association rate constant for the resting conformation, $\sim10^5$ M^{-1}s^{-1}, is unusually low. Even the association rate constant for the flipped conformation, $\sim8 \times 10^6$ M^{-1}s^{-1}, is still slower

than that for the binding of acetylcholine to muscle-type nicotinic receptors, which is $>10^8$ M^{-1}s^{-1}. Although the high affinity ratio (between resting and flipped states) results in a high degree of apparent cooperativity (the Hill slope is close to its maximum value of 2), the absolute value of the flipping equilibrium constant is only near 1, compared with 27 for $\alpha1\beta$ GlyRs (Lape et al., 2008). Nevertheless, the overall efficacy is high because of the high equilibrium constant (E_2) for the shut-open step.

The values of the gating rate constants were the most consistent across experimental sets in our maximum likelihood fitting, regardless of which model was used for fitting. They ranged between 300 and 400 s^{-1} for the shutting rate α and 110,000 and 130,000 s^{-1} for the opening rate β. The values given in Table V for the fit of Scheme 2 have the following implications. The fast opening rate constant is very similar to that for the heteromeric $\alpha1\beta$ receptors (Burzomato et al., 2004), but the shutting rate constant is 20 times slower, so the mean length of the individual openings is ~3 rather than 0.14 ms for heteromeric $\alpha1\beta$ receptors. The mean efficacy for the opening step is ~350, much higher than the gating efficacy of either $\alpha1\beta$ heteromeric GlyR ($\alpha = 7,000$ s^{-1}; $\beta = 129,000$ s^{-1}; $E = 20$) or $\alpha1$ homomeric GlyR ($\alpha = 700$ s^{-1}; $\beta = 28,000$ s^{-1}; $E = 38$; Burzomato et al., 2004). In $\alpha1$-containing receptors, the lower (but still large) efficacy for the open–shut step stems from a faster shutting rate and implies a short mean open time for the $\alpha1$ heteromer, but in the $\alpha1$ homomer, it appears to result from a slower opening rate constant. For $\alpha2$ receptors, the flipping equilibrium constant for saturated receptors (Table V) is around 1, so shut saturated receptors spend about half their time in the resting conformation (A_2R) and half the time flipped (A_2F). The overall effective efficacy is still very high, $E_{eff} = 171$, from Eq. 3, which implies a maximum P_{open} of 99.4%, from Eq. 4.

The energy diagram in Fig. 7 plots the energy barriers for the transitions of fully liganded receptors from resting to flipped to open for the GlyRs we have so far analyzed ($\alpha1$, $\alpha1\beta$, and $\alpha2$). It is interesting to note that the height of the energy barrier that the channel has to cross to go from resting to flipped seems to be linked in our series to whether the principal subunit in the receptor is $\alpha1$ or $\alpha2$. It is plausible that the subunit that provides the principal side of the binding site should play a major part in this transition to flipped, a transition that is likely to correspond to the conformational changes that follow agonist binding and spread through the extracellular domain to reach the channel gate (Grosman et al., 2000; Lee and Sine, 2005). Almost all of the sequence differences between $\alpha1$ and $\alpha2$ are in their extracellular domain, whereas there is only one amino acid difference in M2, the main domain that lines the channel and gates it shut. On the other hand, the M2
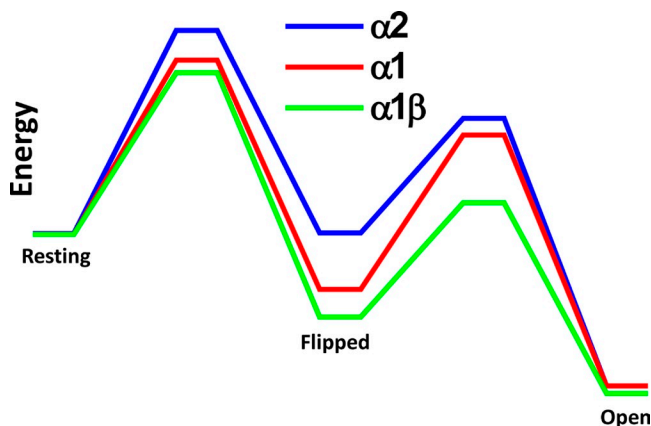
sequence is less conserved in the β subunit. Notably, the energy difference between the initial resting state and the final open state is very similar for the three receptors in the series, corresponding to the fact that the effective efficacy E_{eff} (Eq. 3) of glycine is very high for all three.

The mechanistic interpretation of α2 GlyR bursts

It was shown rigorously by Wyllie et al. (1998; appendix) that the time constants (and mean length) for bursts (activations) measured at sufficiently low agonist concentrations must be the same as the time constants for the decay of macroscopic concentration jumps to zero concentration. Obviously, bursts cannot be measured at zero concentration, so this theorem begs the question, What concentration is "sufficiently low"? For most sorts of receptor, it is possible to record bursts at a concentration that is low enough for there to be good agreement between the single-channel mean burst length and the macroscopic deactivation time constant. According to our interpretation, the α2 receptor is an exception to this rule.

The observed time constant for the predominant slow component of the macroscopic deactivation was 130 ms after a step from 10 mM glycine to zero (Table I). The fit of Scheme 2 predicts a predominant deactivation time constant of 171 ms, not far from that observed. On the other hand, this value does not agree very well with the observed mean burst length of 490 ms measured at the lowest concentration of glycine at which measurements could be made, 20 µM. Evidently, quite a lot of reopening from monoliganded channels must occur at 20 µM glycine, and this reopening prolongs the burst length to a value that is well above its low concentration limit, even at 20 µM glycine. Calculations from the fitted
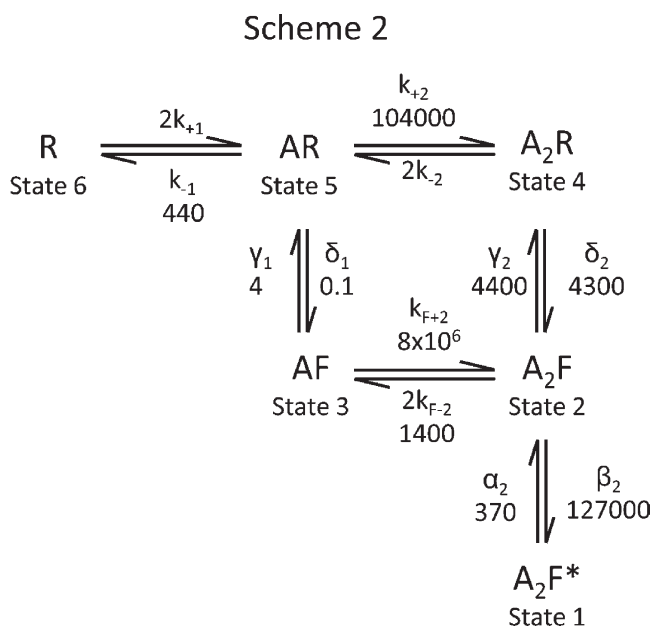
rate constants for Scheme 2 predicts that at a really low glycine concentration, 1 nM, the mean burst length should be 171 ms, in agreement with the predicted deactivation rate for Scheme 2. Clearly, the way the numbers work out in this case makes it impossible to record bursts at a sufficiently low concentration.

To make sense of the numbers, it is useful to define the relative probabilities that a channel moves next to each of the adjacent states in the scheme, regardless of how long it takes to do so. For example, in Scheme 2 (Fig. 8), a monoliganded resting channel AR (state 5) can move next to the resting state, R (state 6), it can flip to AF (state 3), or it can bind another glycine molecule to get to A_2R (state 4). The probabilities are simply proportional to the rate constants for leaving state 5 (Colquhoun and Hawkes, 1995; p. 415), so, for example, the probability that a monoliganded channel dissociates is

$$\pi_{56} = \frac{k_{-1}}{k_{-1} + \delta_1 + k_{+2}c}, \tag{5}$$

where c is the concentration of glycine.

The concentration dependence of the length of an activation arises, in the case of α2 receptors, largely from the binding of glycine to the monoliganded flip state (AF). When 20 µM glycine is applied, opening will take place usually via A_2R because the monoliganded

Scheme 2

Figure 7. Energy diagram for the resting–flipped–open transitions for the fully liganded α1, α1β, and α2 GlyR. Calculations used a frequency factor of 10^{-7} s^{-1} (Andersen, 1999) and the results of the fit of Scheme 2 (flip with two binding sites and one open state) for α2 GlyR, and data from Burzomato et al. (2004) for the α1-containing GlyRs.

Figure 8. Features of Scheme 2 as fitted to α2 GlyR data. The diagram shows the flip mechanism with two binding sites fitted, with the different states numbered to provide a key to the physical interpretation of the results in the Discussion. Numbers above the arrows indicating the transitions are the average rate constants from the fits. Units are s^{-1} or M^{-1}s^{-1}, as appropriate (see Table V).

flipping rate is small (π_{54} π_{42} is almost 20 times greater than π_{53} π_{32}). After an opening, the channel must return to A_2F (state 2), from where it is likely to reopen ($\pi_{21} = 0.96$), but if it does not reopen, it is three times less likely to go to AF (state 3) than to unflip to A_2R.

If this occurs, even at the lowest concentration of glycine for which recordings could be made, 20 µM, the probability that from AF the channel can bind glycine again is high ($\pi_{32} = 0.98$). Because this binding returns the channel to A_2F, and from there the channel is very likely to (re)open, this path accounts for the lengthening of the activation at 20 µM glycine. In contrast to that, the probability of a second binding occurring to the resting conformation, AR, is very low ($\pi_{54} = 0.004$ in 20 µM glycine), and the probability of flipping is even lower.

There are two reasons for the unusually long activations produced by the α2 receptor even at the lowest concentrations. The first is that individual openings are longer, on average, for the α2 receptor (3 ms; Table V) than for the α1β receptor (0.14 ms; Lape et al., 2008). The second reason is the large number of openings per activation seen with the α2 receptor, around 100, even at very low concentrations.

Shut times within an activation turn out to have a rather simple interpretation in the case of the α2 receptor. The distribution of shut times calculated from the fitted rate constants for Scheme 2 (Table V), with Eq. 3.90 from Colquhoun and Hawkes (1982), is dominated at all concentrations by a very short component with a mean of ∼8 µs, close to the mean duration of a sojourn in A_2F (state 2). Clearly, most of the time during an activation is spent oscillating between A_2F^* and A_2F. There is also a small component (a few percent in area) of shut times within activations that has a time constant that is close to the mean lifetime in A_2R (state 4), ∼0.2 ms. This clearly represents channels that undergo transitions $A_2F^* \to A_2F \to A_2R \to A_2F \to A_2F^*$. There will very rarely be oscillations between A_2F and A_2R, so this time constant of the shut-time distribution is close to the time spent in A_2R (plus two brief sojourns in A_2F). Still more rarely (at 20 µM glycine), there will be transitions $A_2F^* \to A_2F \to AF \to A_2F \to A_2F^*$. Again, there will be little oscillation, so these generate a small component of shut times with a mean life close to that in AF. At low concentrations, a channel that after opening reaches AR will very rarely rebind glycine and reopen, but this route will become increasingly common as glycine concentration is increased, and it will contribute to the increase in duration of activations with concentration.

Finally, the shut time between one activation and the next at a low concentration is predicted by the fit to be very long. At 20 µM glycine, the range is 25.6–92.9 s for the three sets used for fitting. The fact that it is so long explains why so few activations could be recorded, and it also explains why the P_{open} is so low (around 0.01) at 20 µM glycine. The shut time between activations is

characterized by at least one sojourn in the resting state, R. However, even at 20 µM glycine, the mean lifetime of a single sojourn in R is quite short, a few hundred milliseconds. So, evidently, there is a lot of oscillation between shut states between one activation and the next. Consider oscillations between the resting state, R (state 6), and the monoliganded resting state, AR (state 5), and back. The distribution of the number of such oscillations can be found as follows. From R, the channel has to reach AR (state 5; i.e., π_{65} is 1). There will be no R–AR oscillations if the channel then moves straight to either state AF (state 3) or A_2R (state 4) without returning to R. Therefore, the probability of there being no R–AR oscillations is $P(0) = \pi_{53} + \pi_{54} = (1 - \pi_{56})$. The probability of one oscillation (R$\to$AR$\to$R$\to$AR$\to$state 3 or 4) must be $P(1) = \pi_{56} (1 - \pi_{56})$. So, in general, the probability of r oscillations between R and AR before leaving for state 3 or state 4 is seen to be

$$P(r) = (\pi_{56})^r (1 - \pi_{56}). \tag{6}$$

These probabilities (from $r = 1$ to ∞) sum to 1, and the mean number of oscillations is

$$\mu_r = \frac{\pi_{56}}{1 - \pi_{56}}. \tag{7}$$

For example, in the fitted set that was used for the histograms, $\pi_{56} = 0.996$ at 20 µM glycine, so the mean number of R$\to$AR$\to$R oscillations is 229. The mean length of a sojourn in R was 251 ms, and the mean length of the monoliganded state AR is 2.17 ms. Thus, the mean length of a run of R$\to$AR$\to$R oscillations is 229 (251 + 2.17) = 58 s. This is almost as long as the mean shut time between activations (74 s in this case). Thus, the very long shut times that separate long activations are due to the many R$\to$AR$\to$R oscillations rather than to the long life of any individual shut state.

REFERENCES

Akagi, H., K. Hirai, and F. Hishinuma. 1991. Cloning of a glycine receptor subtype expressed in rat brain and spinal cord during a specific period of neuronal development. *FEBS Lett.* 281:160–166. doi:10.1016/0014-5793(91)80383-E

Andersen, O.S. 1999. Graphic representation of the results of kinetic analyses. *J. Gen. Physiol.* 114:589–590. doi:10.1085/jgp.114.4.589

Beato, M., P.J. Groot-Kormelink, D. Colquhoun, and L.G. Sivilotti. 2002. Openings of the rat recombinant α1 homomeric glycine receptor as a function of the number of agonist molecules bound. *J. Gen. Physiol.* 119:443–466. doi:10.1085/jgp.20028530

Beato, M., P.J. Groot-Kormelink, D. Colquhoun, and L.G. Sivilotti. 2004. The activation mechanism of α1 homomeric glycine receptors. *J. Neurosci.* 24:895–906. doi:10.1523/JNEUROSCI.4420-03.2004

Becker, C.-M., W. Hoch, and H. Betz. 1988. Glycine receptor heterogeneity in rat spinal cord during postnatal development. *EMBO J.* 7:3717–3726.

Belachew, S., B. Rogister, J.M. Rigo, B. Malgrange, C. Mazy-Servais, G. Xhauflaire, P. Coucke, and G. Moonen. 1998. Cultured oligodendrocyte progenitors derived from cerebral cortex express a glycine receptor which is pharmacologically distinct from the neuronal isoform. *Eur. J. Neurosci.* 10:3556–3564. doi:10.1046/j.1460-9568.1998.00369.x

Burzomato, V., M. Beato, P.J. Groot-Kormelink, D. Colquhoun, and L.G. Sivilotti. 2004. Single-channel behavior of heteromeric α1β glycine receptors: an attempt to detect a conformational change before the channel opens. *J. Neurosci.* 24:10924–10940. doi:10.1523/JNEUROSCI.3424-04.2004

Clements, J.D. 2002. Glycine receptor maturation: no experience required. *J. Physiol.* 542:665. doi:10.1113/jphysiol.2002.025544

Clements, J.D., R.A.J. Lester, G. Tong, C.E. Jahr, and G.L. Westbrook. 1992. The time course of glutamate in the synaptic cleft. *Science.* 258:1498–1501. doi:10.1126/science.1359647

Colquhoun, D., and A.G. Hawkes. 1982. On the stochastic properties of bursts of single ion channel openings and of clusters of bursts. *Philos. Trans. R. Soc. Lond. B Biol. Sci.* 300:1–59. doi:10.1098/rstb.1982.0156

Colquhoun, D., and A.G. Hawkes. 1987. A note on correlations in single ion channel records. *Proc. R. Soc. Lond. B Biol. Sci.* 230:15–52. doi:10.1098/rspb.1987.0008

Colquhoun, D., and A.G. Hawkes. 1990. Stochastic properties of ion channel openings and bursts in a membrane patch that contains two channels: evidence concerning the number of channels present when a record containing only single openings is observed. *Proc. R. Soc. Lond. B Biol. Sci.* 240:453–477. doi:10.1098/rspb.1990.0048

Colquhoun, D., and A.G. Hawkes. 1995. The principles of the stochastic interpretation of ion-channel mechanisms. *In* Single-Channel Recording. B. Sakmann and E. Neher, editors. Plenum Press, New York. 397–482.

Colquhoun, D., P. Jonas, and B. Sakmann. 1992. Action of brief pulses of glutamate on AMPA/kainate receptors in patches from different neurones of rat hippocampal slices. *J. Physiol.* 458:261–287.

Colquhoun, D., A.G. Hawkes, and K. Srodzinski. 1996. Joint distributions of apparent open and shut times of single-ion channels and maximum likelihood fitting of mechanisms. *Philos. Trans. R. Soc. Lond. A.* 354:2555–2590. doi:10.1098/rsta.1996.0115

Colquhoun, D., C.J. Hatton, and A.G. Hawkes. 2003. The quality of maximum likelihood estimates of ion channel rate constants. *J. Physiol.* 547:699–728. doi:10.1113/jphysiol.2002.034165

Edmonds, B., A.J. Gibb, and D. Colquhoun. 1995. Mechanisms of activation of muscle nicotinic acetylcholine receptors and the time course of endplate currents. *Annu. Rev. Physiol.* 57:469–493. doi:10.1146/annurev.ph.57.030195.002345

Flint, A.C., X. Liu, and A.R. Kriegstein. 1998. Nonsynaptic glycine receptor activation during early neocortical development. *Neuron.* 20:43–53. doi:10.1016/S0896-6273(00)80433-X

Fucile, S., D. de Saint Jan, B. David-Watine, H. Korn, and P. Bregestovski. 1999. Comparison of glycine and GABA actions on the zebrafish homomeric glycine receptor. *J. Physiol.* 517:369–383. doi:10.1111/j.1469-7793.1999.0369t.x

Gentet, L.J., and J.D. Clements. 2002. Binding site stoichiometry and the effects of phosphorylation on human α1 homomeric glycine receptors. *J. Physiol.* 544:97–106. doi:10.1113/jphysiol.2001.015321

Grenningloh, G., V. Schmieden, P.R. Schofield, P.H. Seeburg, T. Siddique, T.K. Mohandas, C.-M. Becker, and H. Betz. 1990. Alpha subunit variants of the human glycine receptor: primary structures, functional expression and chromosomal localization of the corresponding genes. *EMBO J.* 9:771–776.

Groot-Kormelink, P.J., M. Beato, C. Finotti, R.J. Harvey, and L.G. Sivilotti. 2002. Achieving optimal expression for single channel recording: a plasmid ratio approach to the expression of α1 glycine receptors in HEK293 cells. *J. Neurosci. Methods.* 113:207–214. doi:10.1016/S0165-0270(01)00500-3

Grosman, C., M. Zhou, and A. Auerbach. 2000. Mapping the conformational wave of acetylcholine receptor channel gating. *Nature.* 403:773–776. doi:10.1038/35001586

Hawkes, A.G., A. Jalali, and D. Colquhoun. 1990. The distributions of the apparent open times and shut times in a single channel record when brief events can not be detected. *Philos. Trans. R. Soc. Lond. A.* 332:511–538. doi:10.1098/rsta.1990.0129

Hawkes, A.G., A. Jalali, and D. Colquhoun. 1992. Asymptotic distributions of apparent open times and shut times in a single channel record allowing for the omission of brief events. *Philos. Trans. R. Soc. Lond. B Biol. Sci.* 337:383–404. doi:10.1098/rstb.1992.0116

Hoch, W., H. Betz, and C.-M. Becker. 1989. Primary cultures of mouse spinal cord express the neonatal isoform of the inhibitory glycine receptor. *Neuron.* 3:339–348. doi:10.1016/0896-6273(89)90258-4

Jones, M.V., and G.L. Westbrook. 1995. Desensitized states prolong GABA$_A$ channel responses to brief agonist pulses. *Neuron.* 15:181–191. doi:10.1016/0896-6273(95)90075-6

Keramidas, A., and N.L. Harrison. 2010. The activation mechanism of α1β2γ2S and α3β3γ2S GABA$_A$ receptors. *J. Gen. Physiol.* 135:59–75. doi:10.1085/jgp.200910317

Langosch, D., L. Thomas, and H. Betz. 1988. Conserved quaternary structure of ligand-gated ion channels: the postsynaptic glycine receptor is a pentamer. *Proc. Natl. Acad. Sci. USA.* 85:7394–7398. doi:10.1073/pnas.85.19.7394

Lape, R., D. Colquhoun, and L.G. Sivilotti. 2008. On the nature of partial agonism in the nicotinic receptor superfamily. *Nature.* 454:722–727.

Lape, R., P. Krashia, D. Colquhoun, and L.G. Sivilotti. 2009. Agonist and blocking actions of choline and tetramethylammonium on human muscle acetylcholine receptors. *J. Physiol.* 587:5045–5072. doi:10.1113/jphysiol.2009.176305

Lee, W.Y., and S.M. Sine. 2005. Principal pathway coupling agonist binding to channel gating in nicotinic receptors. *Nature.* 438:243–247. doi:10.1038/nature04156

Legendre, P. 2001. The glycinergic inhibitory synapse. *Cell. Mol. Life Sci.* 58:760–793. doi:10.1007/PL00000899

Lewis, T.M., P.R. Schofield, and A.M. McClellan. 2003. Kinetic determinants of agonist action at the recombinant human glycine receptor. *J. Physiol.* 549:361–374. doi:10.1113/jphysiol.2002.037796

Malosio, M.L., B. Marquèze-Pouey, J. Kuhse, and H. Betz. 1991. Widespread expression of glycine receptor subunit mRNAs in the adult and developing rat brain. *EMBO J.* 10:2401–2409.

Mangin, J.M., A. Guyon, D. Eugène, D. Paupardin-Tritsch, and P. Legendre. 2002. Functional glycine receptor maturation in the absence of glycinergic input in dopaminergic neurones of the rat substantia nigra. *J. Physiol.* 542:685–697. doi:10.1113/jphysiol.2002.018978

Mangin, J.M., M. Baloul, L. Prado De Carvalho, B. Rogister, J.M. Rigo, and P. Legendre. 2003. Kinetic properties of the α2 homo-oligomeric glycine receptor impairs a proper synaptic functioning. *J. Physiol.* 553:369–386. doi:10.1113/jphysiol.2003.052142

Meyer, G., J. Kirsch, H. Betz, and D. Langosch. 1995. Identification of a gephyrin binding motif on the glycine receptor β subunit. *Neuron.* 15:563–572. doi:10.1016/0896-6273(95)90145-0

Mukhtasimova, N., W.Y. Lee, H.L. Wang, and S.M. Sine. 2009. Detection and trapping of intermediate states priming nicotinic receptor channel opening. *Nature.* 459:451–454. doi:10.1038/nature07923

Nguyen, L., B. Malgrange, S. Belachew, B. Rogister, V. Rocher, G. Moonen, and J.M. Rigo. 2002. Functional glycine receptors are expressed by postnatal nestin-positive neural stem/progenitor cells. *Eur. J. Neurosci.* 15:1299–1305. doi:10.1046/j.1460-9568.2002.01966.x

Pitt, S.J., L.G. Sivilotti, and M. Beato. 2008. High intracellular chloride slows the decay of glycinergic currents. *J. Neurosci.* 28:11454–11467. doi:10.1523/JNEUROSCI.3890-08.2008

Plested, A.J., P.J. Groot-Kormelink, D. Colquhoun, and L.G. Sivilotti. 2007. Single-channel study of the spasmodic mutation α1A52S in recombinant rat glycine receptors. *J. Physiol.* 581:51–73. doi:10.1113/jphysiol.2006.126920

Rayes, D., M.J. De Rosa, S.M. Sine, and C. Bouzat. 2009. Number and locations of agonist binding sites required to activate homomeric Cys-loop receptors. *J. Neurosci.* 29:6022–6032. doi:10.1523/JNEUROSCI.0627-09.2009

Sakmann, B., J. Patlak, and E. Neher. 1980. Single acetylcholine-activated channels show burst-kinetics in presence of desensitizing concentrations of agonist. *Nature.* 286:71–73. doi:10.1038/286071a0

Singer, J.H., E.M. Talley, D.A. Bayliss, and A.J. Berger. 1998. Development of glycinergic synaptic transmission to rat brain stem motoneurons. *J. Neurophysiol.* 80:2608–2620.

Takahashi, T., A. Momiyama, K. Hirai, F. Hishinuma, and H. Akagi. 1992. Functional correlation of fetal and adult forms of glycine receptors with developmental changes in inhibitory synaptic receptor channels. *Neuron.* 9:1155–1161. doi:10.1016/0896-6273(92)90073-M

Twyman, R.E., and R.L. Macdonald. 1991. Kinetic properties of the glycine receptor main- and sub-conductance states of mouse spinal cord neurones in culture. *J. Physiol.* 435:303–331.

Watanabe, E., and H. Akagi. 1995. Distribution patterns of mRNAs encoding glycine receptor channels in the developing rat spinal cord. *Neurosci. Res.* 23:377–382. doi:10.1016/0168-0102(95)00972-V

Wyllie, D.J., P. Béhé, and D. Colquhoun. 1998. Single-channel activations and concentration jumps: comparison of recombinant NR1a/NR2A and NR1a/NR2D NMDA receptors. *J. Physiol.* 510:1–18. doi:10.1111/j.1469-7793.1998.001bz.x